

## LA-UR-20-27819

Approved for public release; distribution is unlimited.

Title: MCNP Reactor Multigroup Tally Options Verification

Author(s): Wilkerson, Robert Blake  
McKinney, Gregg  
Rising, Michael Evan  
Kulesza, Joel A.

Intended for: Report

Issued: 2020-10-02 (Draft)

---

**Disclaimer:**

Los Alamos National Laboratory, an affirmative action/equal opportunity employer, is operated by Triad National Security, LLC for the National Nuclear Security Administration of U.S. Department of Energy under contract 89233218CNA000001. By approving this article, the publisher recognizes that the U.S. Government retains nonexclusive, royalty-free license to publish or reproduce the published form of this contribution, or to allow others to do so, for U.S. Government purposes. Los Alamos National Laboratory requests that the publisher identify this article as work performed under the auspices of the U.S. Department of Energy. Los Alamos National Laboratory strongly supports academic freedom and a researcher's right to publish; as an institution, however, the Laboratory does not endorse the viewpoint of a publication or guarantee its technical correctness.

# **MCNP Reactor Multigroup Tally Options Verification**

Blake Wilkerson, Gregg W. McKinney, Michael E. Rising, Joel Kulesza

Los Alamos National Laboratory

## 1 Multigroup Tally Options

### 1.1 Introduction

For the next release of the MCNP6 code version 6.3, several new multigroup (MG) special treatment tally options have also been implemented and tested. These new special tally treatment options have been developed to facilitate the production of transport parameters that characterize the transmission and scatter of neutrons within a material region. In a MG form, the cross sections can be used for more computationally efficient Monte Carlo or deterministic transport calculations as well as for diffusion, reactor kinetics and other multi-physics simulations. While these tally options currently apply only to neutron transport (i.e., f4:n tallies), there is no reason this implementation couldn't be extended to other particle types. A brief description of each of these options is provided in the following subsections, followed by Sections 2-4 that present examples and verification results.

### 1.2 Multigroup Cross Sections (MGC)

The FT MGC special tally option automatically generates ten FM multiplier bins that tally the flux and nine flux-weighted quantities of interest to multigroup transport, using the energy bin structure specified on a related energy bin (E0 or En) card. This tally option can only be used with F4 tallies. The optional UF entry specifies microscopic cross-section units (barns) by default (i.e., when unspecified or set to "0") or macroscopic units (1/cm) when non-zero. When output (to the OUTP file, plotting, or MCTAL file), the flux-weighted quantities are divided by the flux values to produce multigroup cross sections and transport parameters. These FM4 bins are tallied for each cell listed on the related F4 card, and a full description of each bin is provided, as usual, in Table 30 of the OUTP file, along with a condensed description in the tally output tables. The ten multiplier bins are given in Table 1.

Table 1: Multiplier Bins in New MGC Tally

<b>Bin #</b>	<b>Unit</b>	<b>Values</b>
<b>1</b>	neutrons/cm <sup>2</sup> ·s	<i>Flux</i>
<b>2</b>	shakes/cm	<i>Inverse velocity</i>
<b>3</b>	barns	<i>Total cross section</i>
<b>4</b>	barns	<i>Capture cross section</i>
<b>5</b>	barns	<i>Fission cross section</i>
<b>6</b>	barns	<i>Total/prompt fission production cross section</i>
<b>7</b>	barns	<i>Delayed fission production cross section</i>
<b>8</b>	MeV-barns	<i>Fission heat production cross section</i>
<b>9</b>	barns	<i>Absorption (capture + fission) cross section</i>
<b>10</b>	barns	<i>Scatter (total - absorption) cross section</i>

As usual, these FM tally bins can be viewed with the tally plotter using the “free e” and “fix m 2” options, along with the “nonorm” keyword to disable the automatic division by the energy bin widths (see examples in Section 2.1).

### 1.3 Scatter Probability Matrices (SPM)

The FT SPM special tally option generates collision exit energy-angle scatter probability matrices averaged over particle interactions within each incident energy bin defined with the tally user (FU) bins. The FU bins are automatically created from and identical to the bins specified on a related energy (E0 or En) card. This tally option can only be used with F4 tallies. The required NA entry specifies the number of uniform cosine bins that will be generated on the related cosine (C4) card (from -1 to 1). This option requires analog transport, and the SPMs are tallied for each cell listed on the related F4 card. Fission neutrons are omitted from the SPM, however, subsequent collisions after fission are included. The SPMs are normalized to the number of collisions contributing to that exit energy-angle SPM, thus the total E-bin/C-bin for each FU-bin equals one. Consider using the tally output (FQ4) card with order “e c” to get exit cosine bins listed horizontally and energy bins listed vertically.

SPMs are independent of the source specification, although a poor choice in the source energy distribution may result in poor SPM convergence or no SPM results for some incident energies. SPM energy-angle contour plots can be generated in the tally plotter using the “free ec” option, along with the “fix u 1” option to specify the incident energy bin (see examples in Section 2.2).

### 1.4 Legendre Coefficients for Scatter (LCS)

The FT LCS special tally option generates Legendre coefficients for scattering cross-section expansions averaged over collisions within each incident energy bin defined with the tally user (FU) bins. The FU user bins are automatically created from and identical to the bins specified on a related energy bins (E0 or En) card. This tally option can only be used with F4 tallies. The required LO entry specifies the Legendre order and thus the number of coefficients that will be generated on the related cosine bin (C4) card, in addition to the scatter bin’s normalization factor (i.e., fraction of collisions contributing to the related coefficients). The C4 bins are labeled as 0.00 (norm. factor), 1.00 (1st coeff.), 2.00 (2nd coeff.), etc. These coefficients can be combined with the Legendre polynomials to approximately reproduce the scatter distributions produced with the FT SPM option. This tally option requires analog transport, and the Legendre coefficients are tallied for each cell listed on the related F4 card. Fissions are not included as a scatter event.

The LCS tally values can be combined with the Legendre polynomials,  $P_i(\mu)$ , to obtain the scatter function for any given incident energy  $E'$ , outgoing energy  $E$  bin, using

$$F(\mu) \cong \sum_{i=0}^N a_i P_i(\mu)$$

where

$$a_0 = \frac{1}{2}, \quad a_i = \frac{2i+1}{2} \int_{-1}^1 p(\mu) P_i(\mu) d\mu$$

and  $p(\mu)$  is the probability for scatter angle  $\mu$ . This tally option scores the integral term of this equation; thus these tally values should be multiplied by the  $(2i + 1)/2$  factor to obtain the  $a_i$

coefficients. The integral term is formed in typical Monte Carlo fashion by averaging N samples to obtain

$$\langle P_i \rangle = \frac{1}{N} \sum_{n=1}^N P_i(\mu_n)$$

Note, since  $P_1(\mu) = \mu$ , then  $\langle P_1 \rangle = \langle \mu \rangle$  which is listed as the first tally value (labeled as cosine bin 1.00). The MCNP tally implementation for higher-order terms, found in subroutine TALLY.F90, uses the recursion formula

$$P_{n+1}(\mu) = \frac{1}{n+1} [(2n+1)\mu P_n(\mu) - nP_{n-1}(\mu)]$$

to evaluate the Legendre polynomials.

### 1.5 Induced Fission Neutron Spectra (FNS)

The FT FNS special tally option generates fission neutron spectra averaged over neutron induced fissions within each incident energy bin defined with the tally user (FU) bins. The FU user bins are automatically created from and identical to the bins specified on a related energy bin (E0 or En) card. This tally option can only be used with F4 tallies. The optional NT entry specifies the number of uniform half-life bins (from 100 to  $10^{11}$  sh) that will be generated on the related time bin (T4) card for prompt (1<sup>st</sup> bin) and delayed (remaining NT bins) fission neutrons. A value of NT=6 results in a prompt bin (100 sh) and the standard six ENDF delayed half-life bins (with midpoints of  $1.79 \times 10^8$ ,  $4.96 \times 10^7$ ,  $2.230 \times 10^8$ ,  $6.000 \times 10^8$ ,  $2.1840 \times 10^9$ ,  $5.4510 \times 10^9$  sh). If NT is not specified, a T4 card must be used to list the prompt and delayed bin boundaries. This tally option requires analog transport, and the FNS are tallied for each cell listed on the related F4 card.

For fixed-source problems, libraries and/or models can be specified to generate the delayed neutrons (see ACT card), while KCODE problems only use libraries for delayed neutron production. These spectra can be viewed in the tally plotter using the “free e” and “fix u 1 fix t 1” options, with the latter specifying the incident energy bin and desired prompt/delayed time bin.

## 2 Multigroup Tally Examples

The following sections provide qualitative verification details for each of the new tally options.

### 2.1 MGC Example

The MCNP input file listing with the MGC option for a 100-cm radius sphere of water with U-235, split into two halves:

```

Test MGC tally option
1 1 -1.0 -1 2 imp:n=1
2 1 -1.0 -1 -2 imp:n=1
3 0 1 imp:n=0

```

```

1 so 100.0
2 px 0.0

m1 1001 2 8016 1 92235 0.0003
cut:n 2j 0 0
sdef pos=.01 0 0
f4:n 1 2
ft4 mgc
e4 1e-8 29log 20.
f14:n 1 2
e14 1e-8 29log 20.
nps 1000000
prdmp 2j 1
print

```

Table 30 in the related MCNP output file, listing the created multiplier bins:

```

ltally      4                                print table 30
      tally type 4  track length estimate of particle flux.
      particle(s): neutrons
cells      1 2

```

```

multiplier bins
att constant  material  reactions or material-rho*x pairs
1.00000E+00
1.00000E+00  1/velocity
1.00000E+00   0   -1
1.00000E+00   0   -2
1.00000E+00   0   -6
1.00000E+00   0   -6  -7
1.00000E+00   0   -6  -9
1.00000E+00   0   -6  -8
1.00000E+00   0   -2  :  -6
1.00000E+00   0   -1  #  -2  #  -6

```

Figures 1-4 show the MGC tally results for all ten multiplier bins.

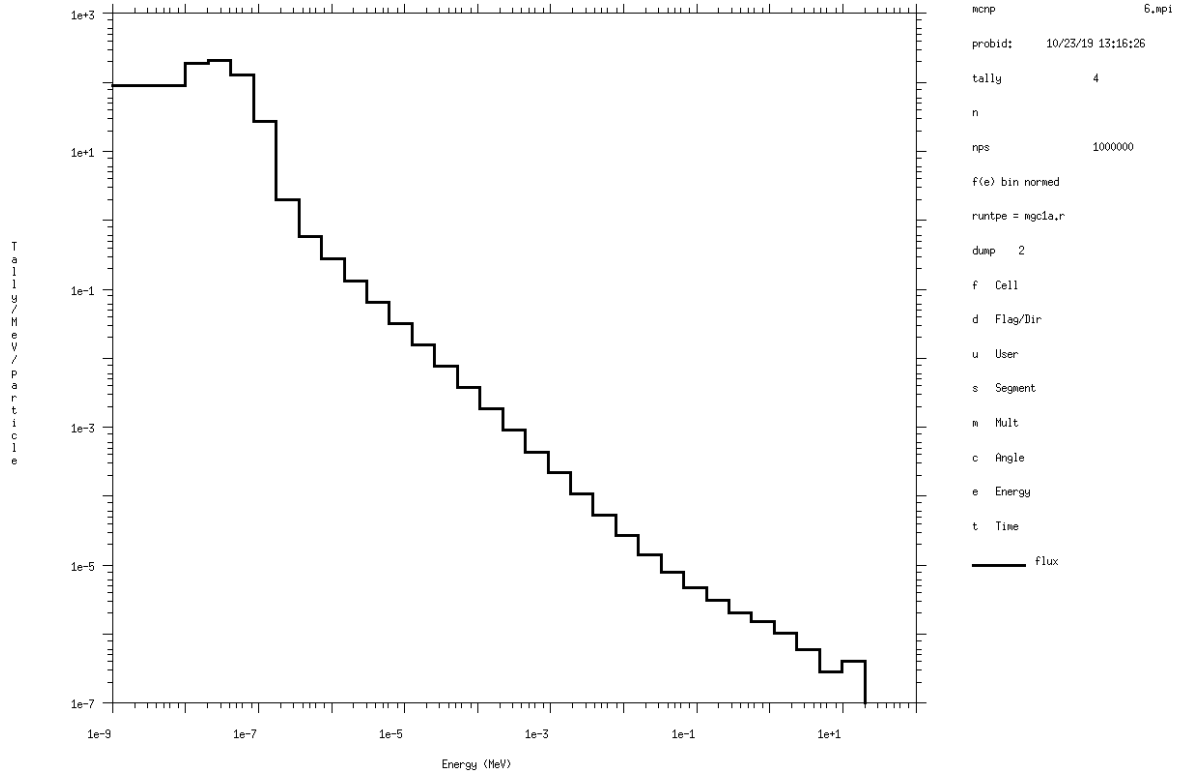


Figure 1. MCNP plot of the flux in 1st multiplier bin.

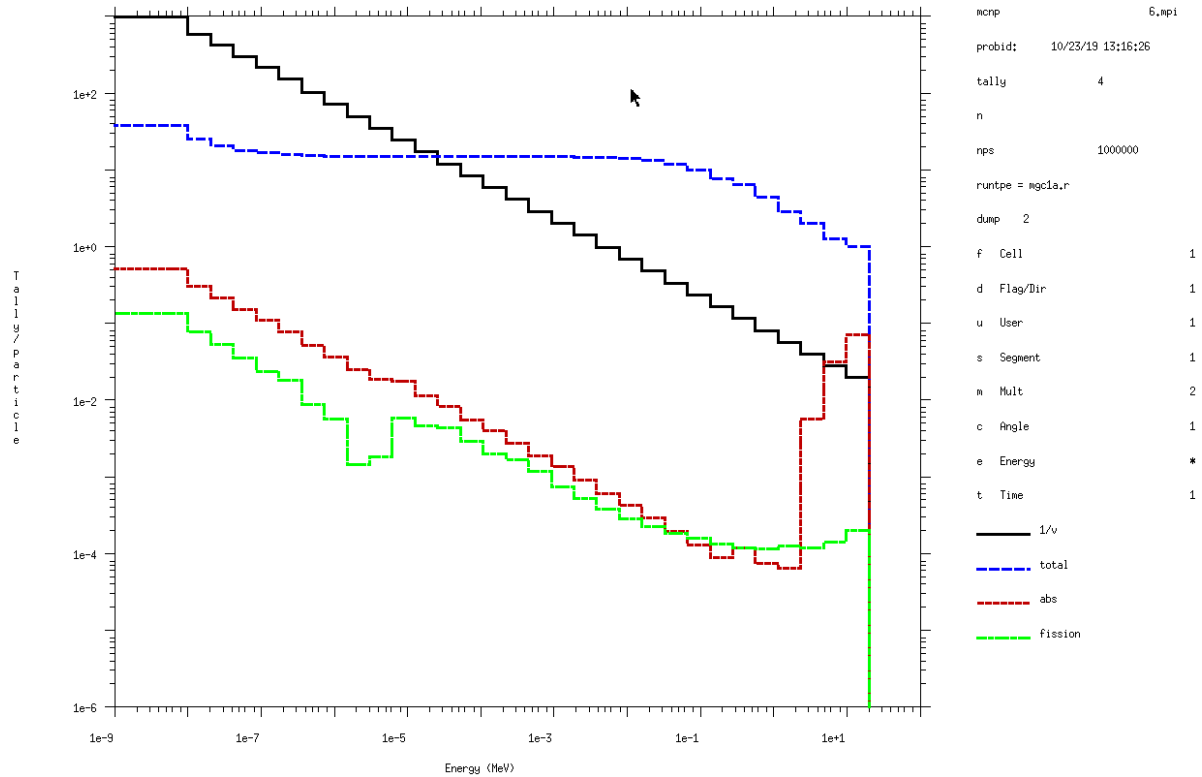


Figure 2. MCNP plots of the next four multiplier bins:  $1/v$  (black), total (blue), capture (red), and fission (green) multigroup cross sections.

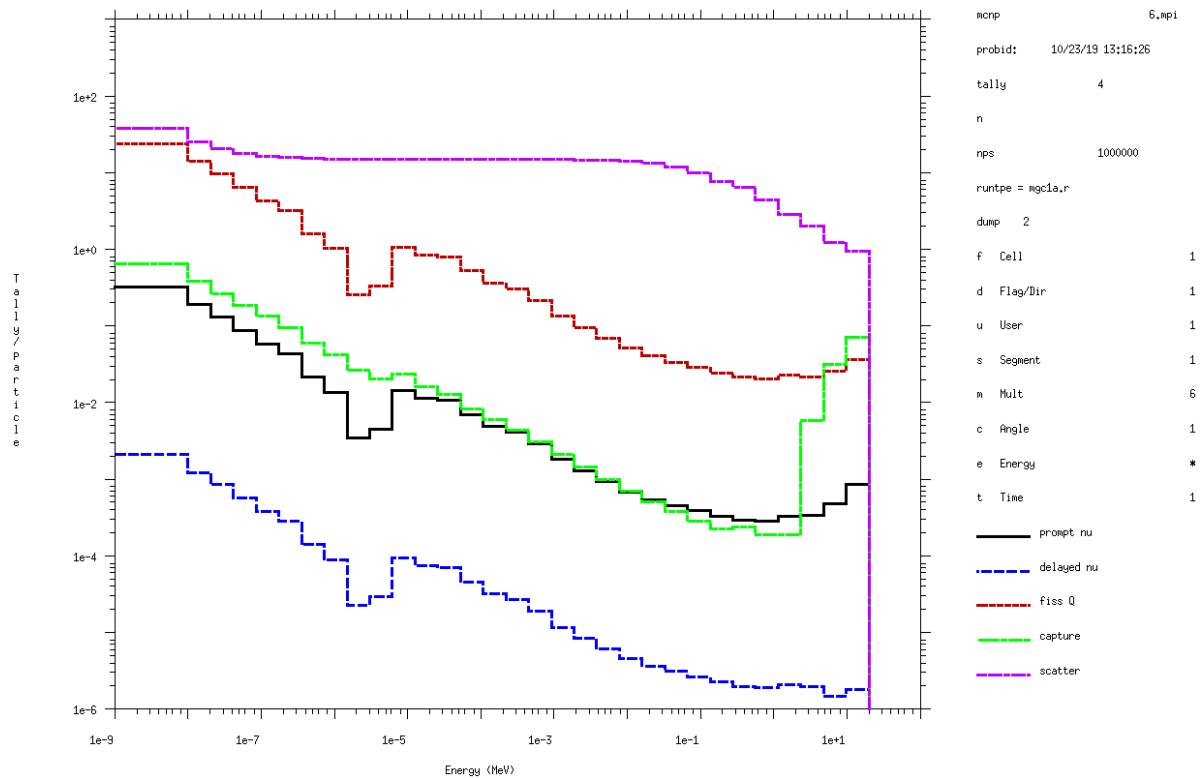


Figure 3. MCNP plots for the remaining five multiplier bins: prompt neutron production (black), delayed neutron production (blue), fission heating (red), absorption (green), and scatter (magenta) multigroup cross sections.

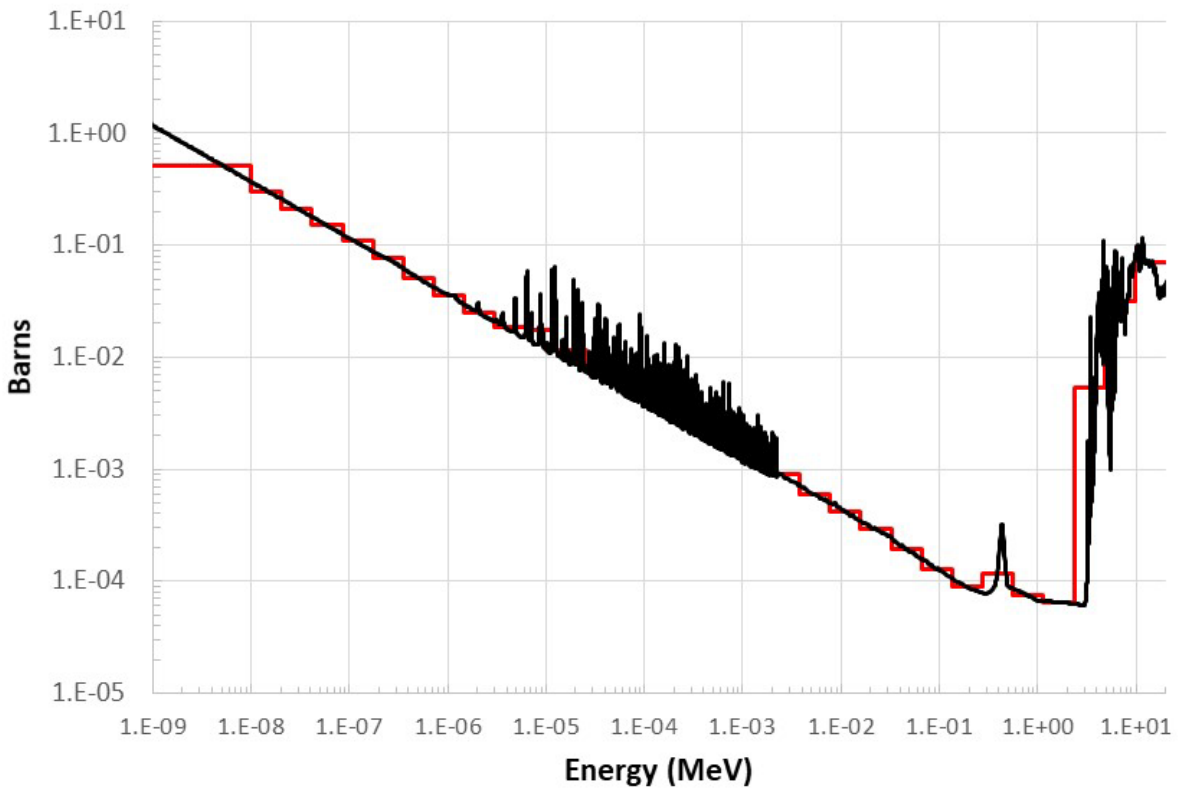


Figure 4. Comparison of the ACE capture cross section (black) to the MGC capture cross section (red), where the ACE data are plotted for the material used in this example ( $H_2O+^{235}U$ ). This plot provides qualitative verification of the MGC tally option.

## 2.2 SPM Example

The MCNP input file listing with the SPM option for a 100-cm radius sphere of water, split into two halves:

```
Test SPM tally option
1 1 -1.0 -1 2 imp:n=1
2 1 -1.0 -1 -2 imp:n=1
3 0 1 imp:n=0

1 so 100.0
2 px 0.0

m1 1001 2 8016 1
cut:n 2j 0 0
sdef pos=.01 0 0
f4:n 1 2
ft4 spm 20
e4 1e-8 29log 20.
fq4 e c
nps 1000000000
print
```

Figures 5-8 show MCNP contour plots of the SPMs for four incident neutron energy groups (each SPM sums to unity). These provide qualitative verification for the SPM tally option, but comparisons to the LCS tally option in the following section are more compelling.

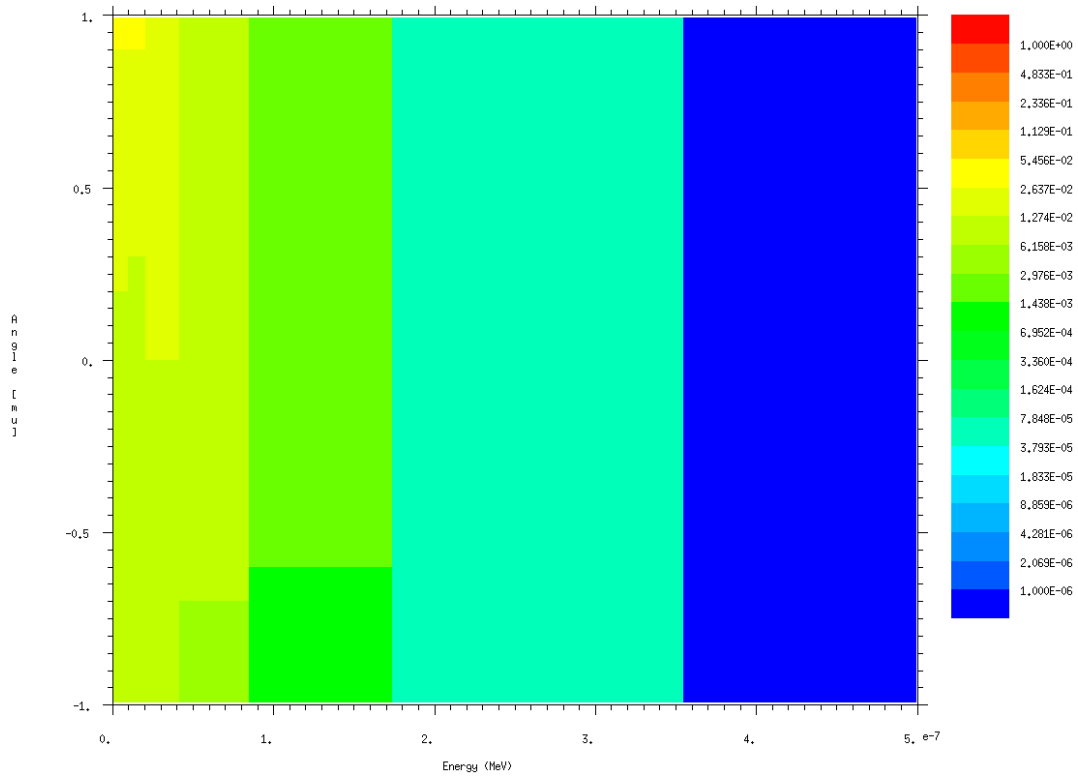


Figure 5. Incident energy from  $0-1 \times 10^{-8}$  MeV (1st FU bin).

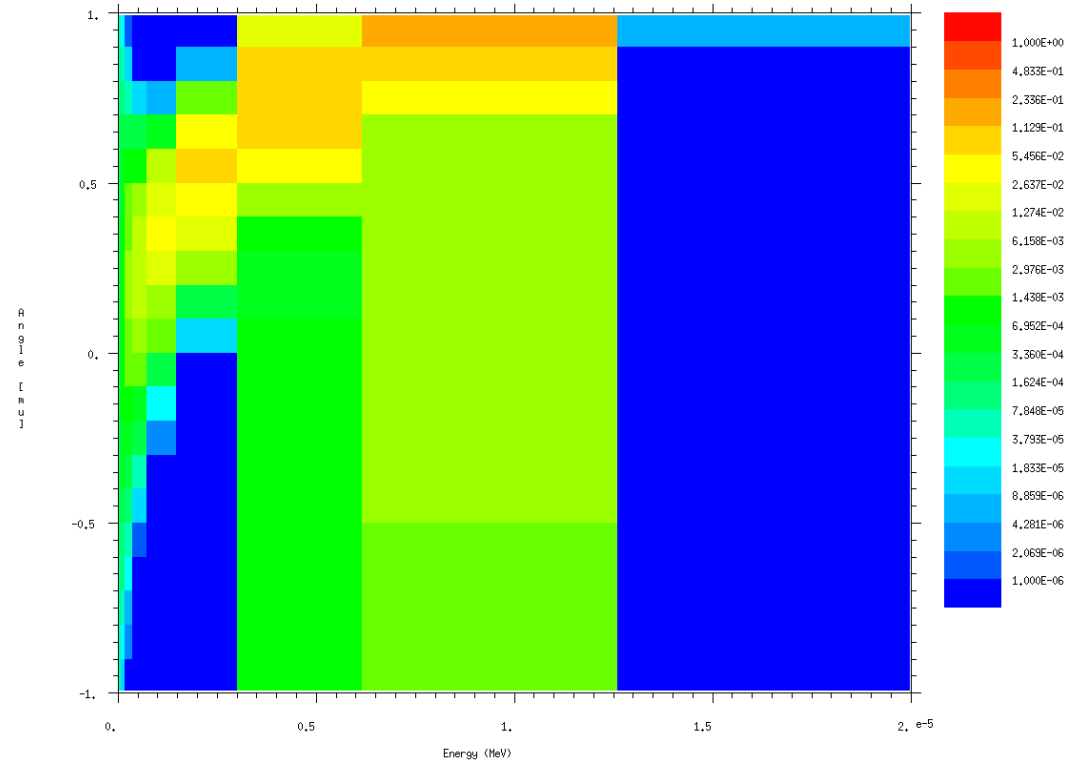


Figure 6. Incident energy from  $6.17 \times 10^{-6}-1.26 \times 10^{-5}$  MeV (11th FU bin).

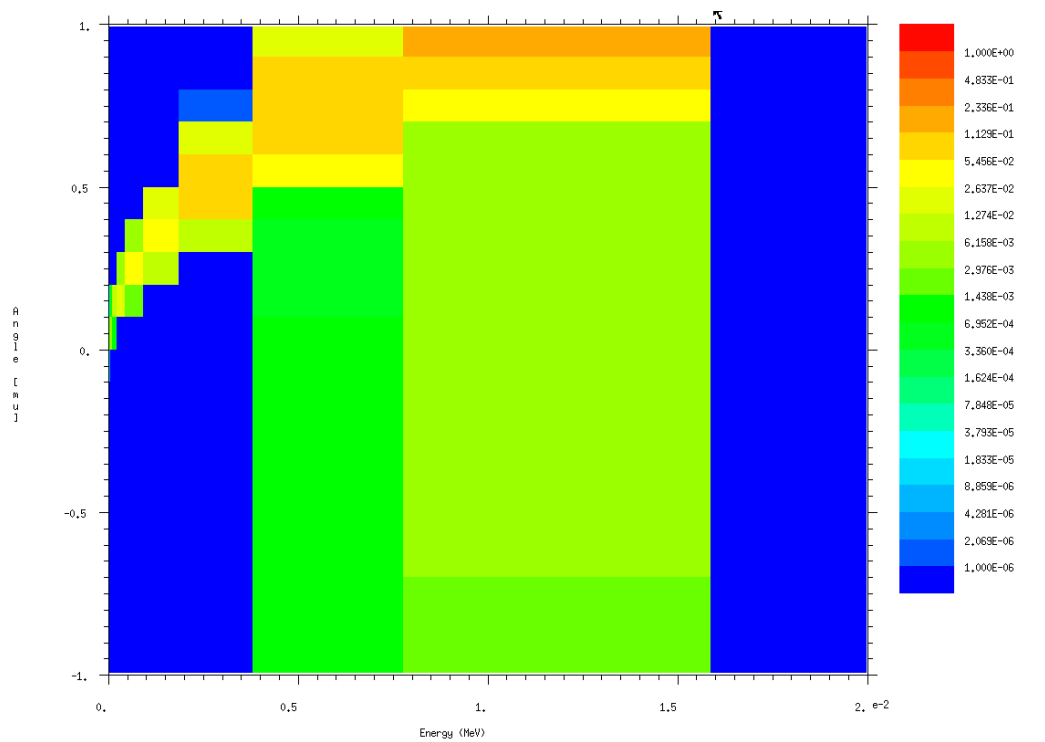


Figure 7. Incident energy from  $7.77 \times 10^{-3}$ - $1.59 \times 10^{-2}$  MeV (21st FU bin)

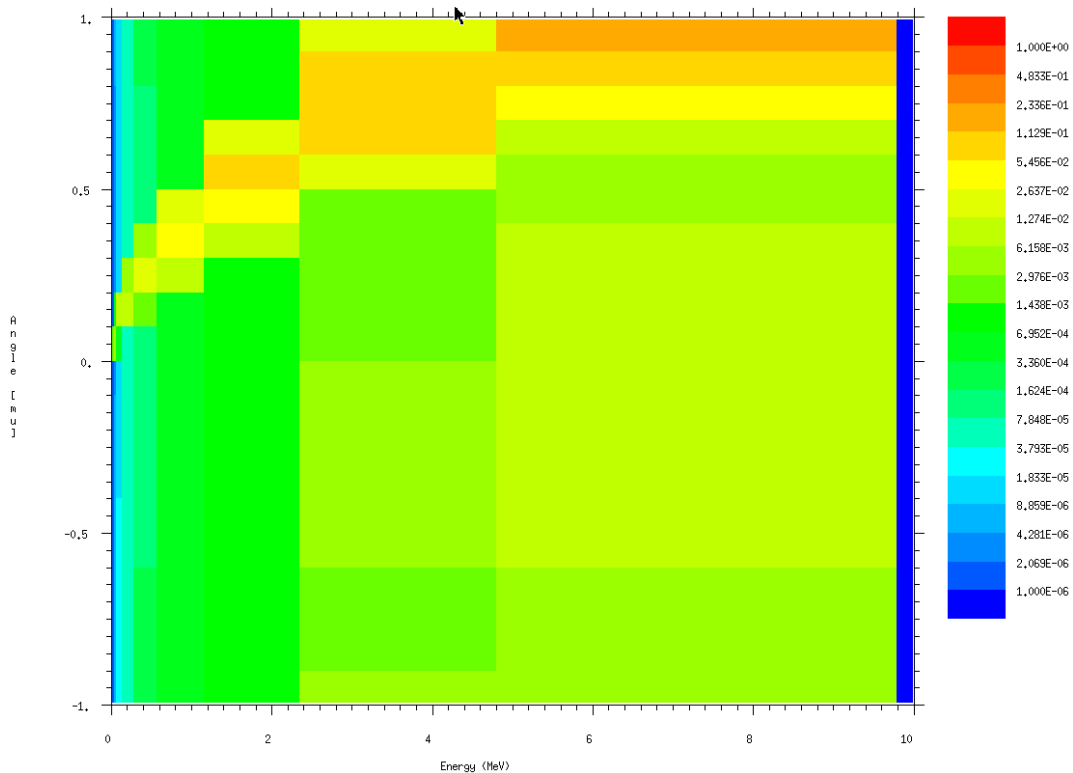


Figure 8. Incident energy from 4.80-9.79 MeV (30th FU bin).

### 2.3 LCS Example

The MCNP input file listing with the LCS option for a 100-cm radius sphere of water, split into two halves:

```
Test LCS tally option
1 1 -1.0 -1 2 imp:n=1
2 1 -1.0 -1 -2 imp:n=1
3 0 1 imp:n=0

1 so 100.0
2 px 0.0

m1 1001 2 8016 1
cut:n 2j 0 0
sdef pos=.01 0 0
e0 1e-8 29log 20.
f4:n 1 2
ft4 lcs 8
fq4 e c
fl4:n 1 2
ft14 spm 40
fq14 c e
nps 1000000000
print
```

Figures 9-11 compare Legendre fits, by expanding the  $F(\mu)$  function to the actual MCNP SPM tallies.

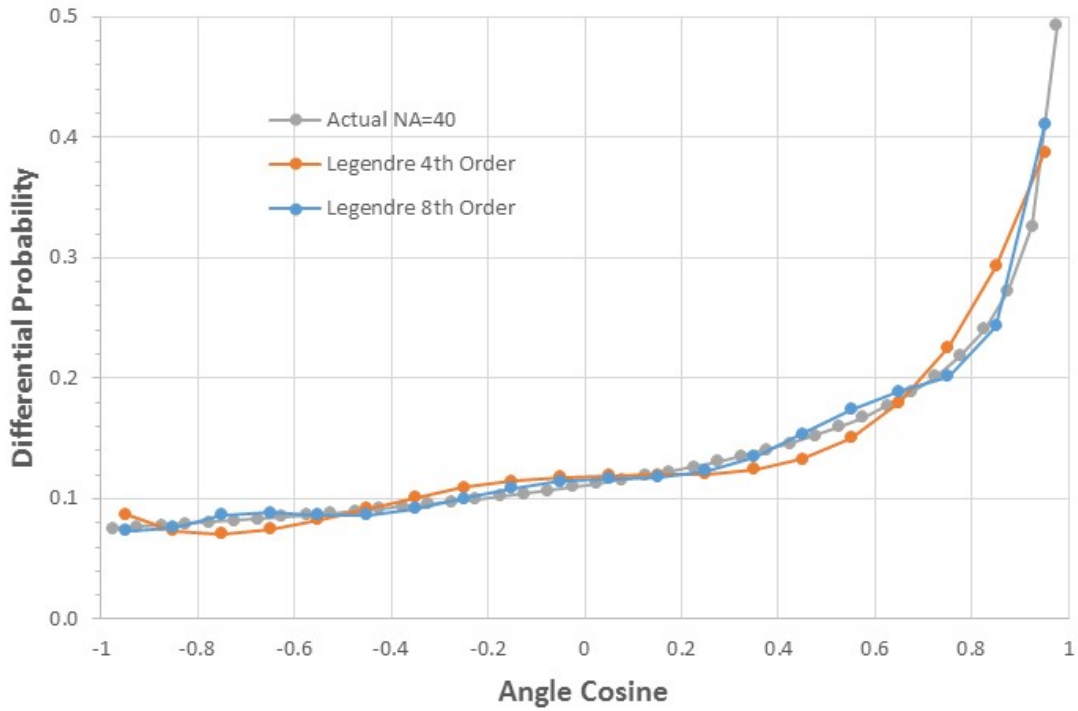


Figure 9. Comparison of the Legendre fit to the MCNP SPM tally for the 1st incident energy bin ( $0-1 \times 10^{-8}$  MeV) and 1st outgoing energy bin ( $0-1 \times 10^{-8}$  MeV).

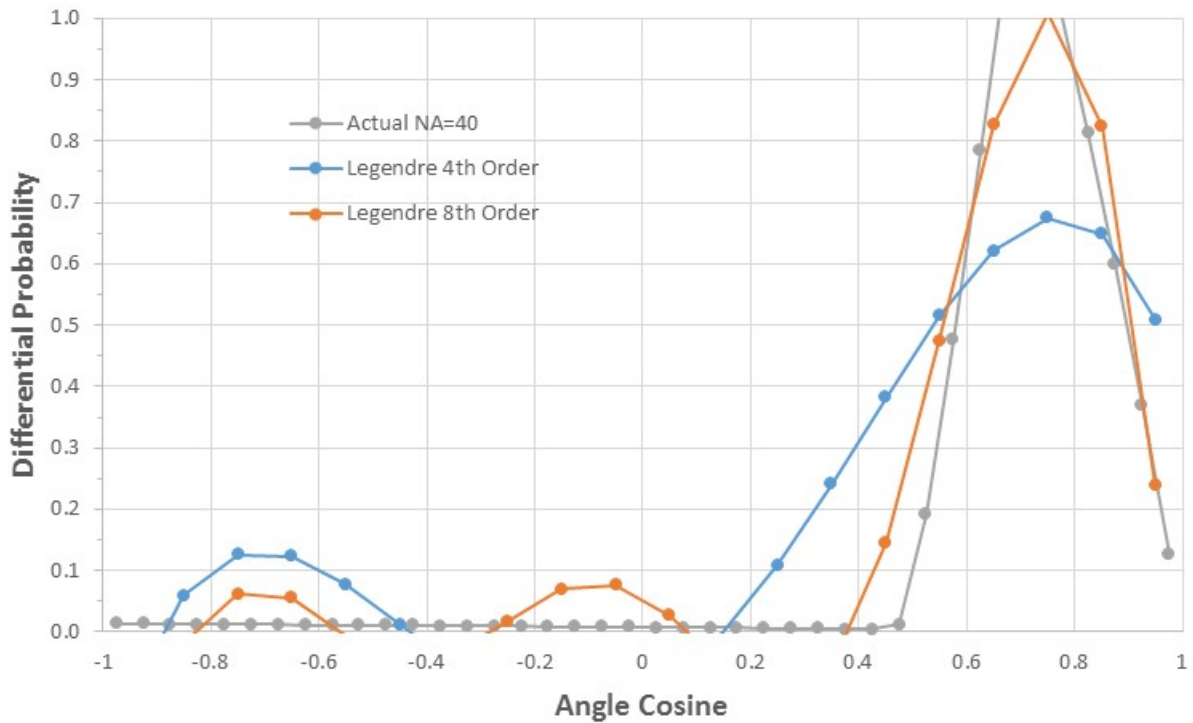


Figure 10. Comparison of the Legendre fit to the MCNP SPM tally for the 18th incident energy bin ( $4.47 \times 10^{-4} - 9.13 \times 10^{-4}$  MeV) and 17th outgoing energy bin ( $2.19 \times 10^{-4} - 4.47 \times 10^{-4}$  MeV).

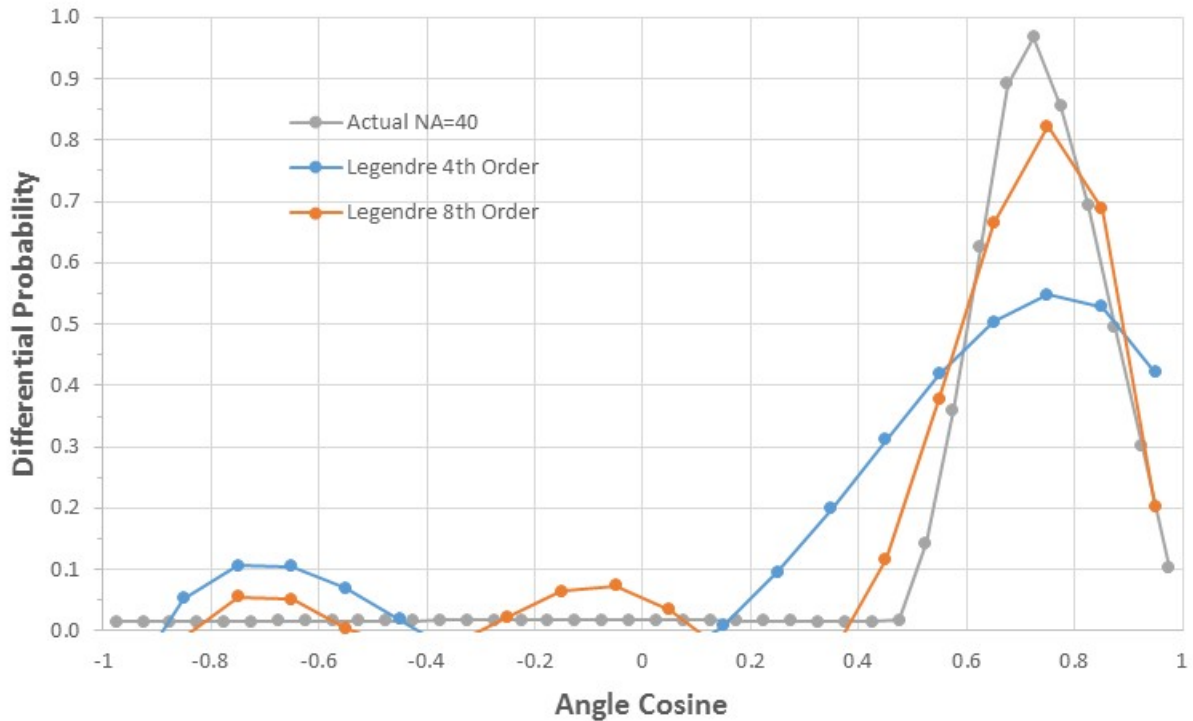


Figure 11. Comparison of the Legendre fit to the MCNP SPM tally for the 28th incident energy bin (0.56-1.15 MeV) and 27th exit energy bin (0.28-0.56 MeV).

The comparison plots in Figs. 9-11 provide verification of the consistency between the SPM and LCS tally options, in that as the Legendre order is increased the agreement improves dramatically (although in some cases a Legendre order of 16 or higher may be required).

## 2.4 FNS Example

The MCNP input file listing with the FNS option for a 100-cm radius sphere of water, split into two halves, with  $^{235}\text{U}$ :

```

Test FNS tally option
1 1 -1.0 -1 2 imp:n=1
2 1 -1.0 -1 -2 imp:n=1
3 0 1 imp:n=0

1 so 100.0
2 px 0.0

m1 1001 2 8016 1 92235 0.0001
cut:n 2j 0 0
sdef pos=.01 0 0
f4:n 1 2

```

```

ft4 fns 6
e4 1e-8 29log 20.
fl4:n 1 2
e14 1e-8 29log 20.
nps 1000000000
print

```

Table 30 in the related MCNP output file, listing the created multiplier bins:

```

ltally      4                                print table 30
  tally type 4  track length estimate of particle flux.
  particle(s): neutrons
cells      1 2

```

```

user bins 1.00000E-08 2.04190E-08 4.16935E-08 8.51340E-08 1.73835E-07 3.54954E-07
7.24780E-07 1.47993E-06
          3.02186E-06 6.17034E-06 1.25992E-05 2.57263E-05 5.25306E-05 1.07262E-04
2.19018E-04 4.47214E-04
          9.13165E-04 1.86459E-03 3.80731E-03 7.77414E-03 1.58740E-02 3.24131E-02
6.61844E-02 1.35142E-01
          2.75946E-01 5.63454E-01 1.15052E+00 2.34924E+00 4.79691E+00 9.79480E+00
2.00000E+01 total

```

```

energy bins
  0.00000E+00 to 1.00000E-08 MeV
  1.00000E-08 to 2.04190E-08 MeV
  2.04190E-08 to 4.16935E-08 MeV
  4.16935E-08 to 8.51340E-08 MeV

```

...

```

time bins
-i      to 1.00000E+02 shakes
  1.00000E+02 to 3.37500E+07 shakes
  3.37500E+07 to 1.36300E+08 shakes
  1.36300E+08 to 4.11500E+08 shakes
  4.11500E+08 to 1.39200E+09 shakes
  1.39200E+09 to 3.81750E+09 shakes
  3.81750E+09 to 1.63530E+10 shakes
total bin

```

Figures 12 and 13 show MCNP plots of the prompt and delayed neutron spectra, respectively.

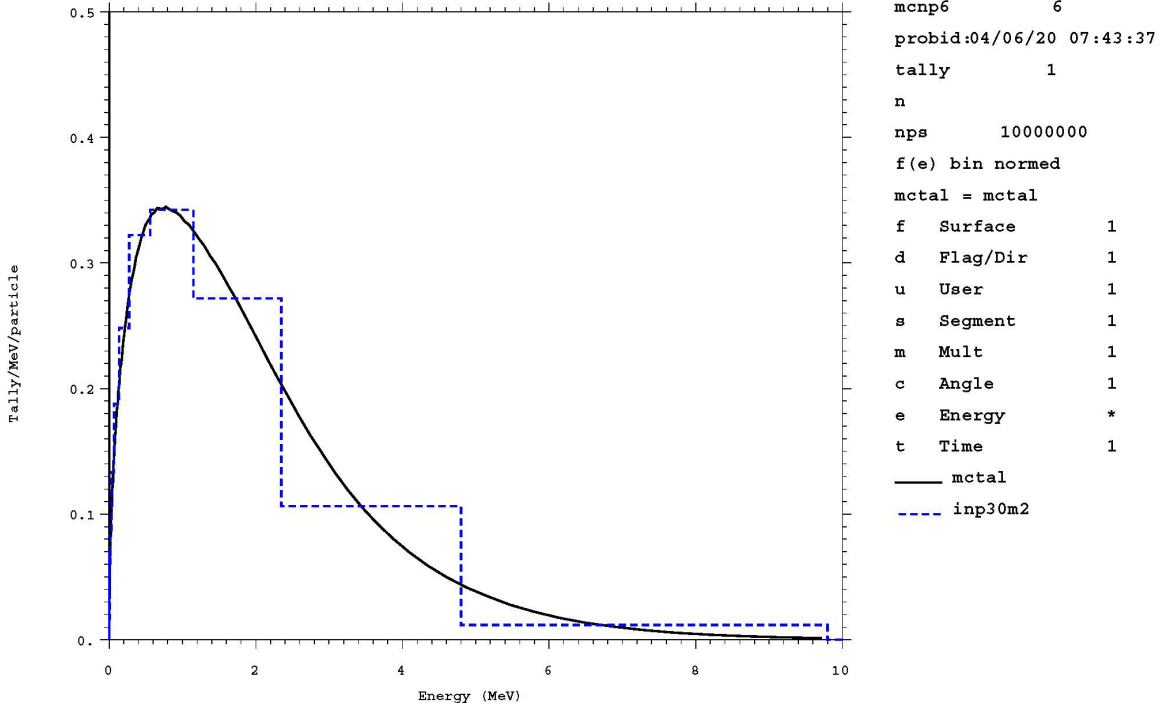


Figure 12. The prompt ACE (black) and FNS (blue) neutron spectra for the 1st incident energy bin (0.0-1e0-8 MeV). Note the FNS integral is  $1-\beta=.9935$ .

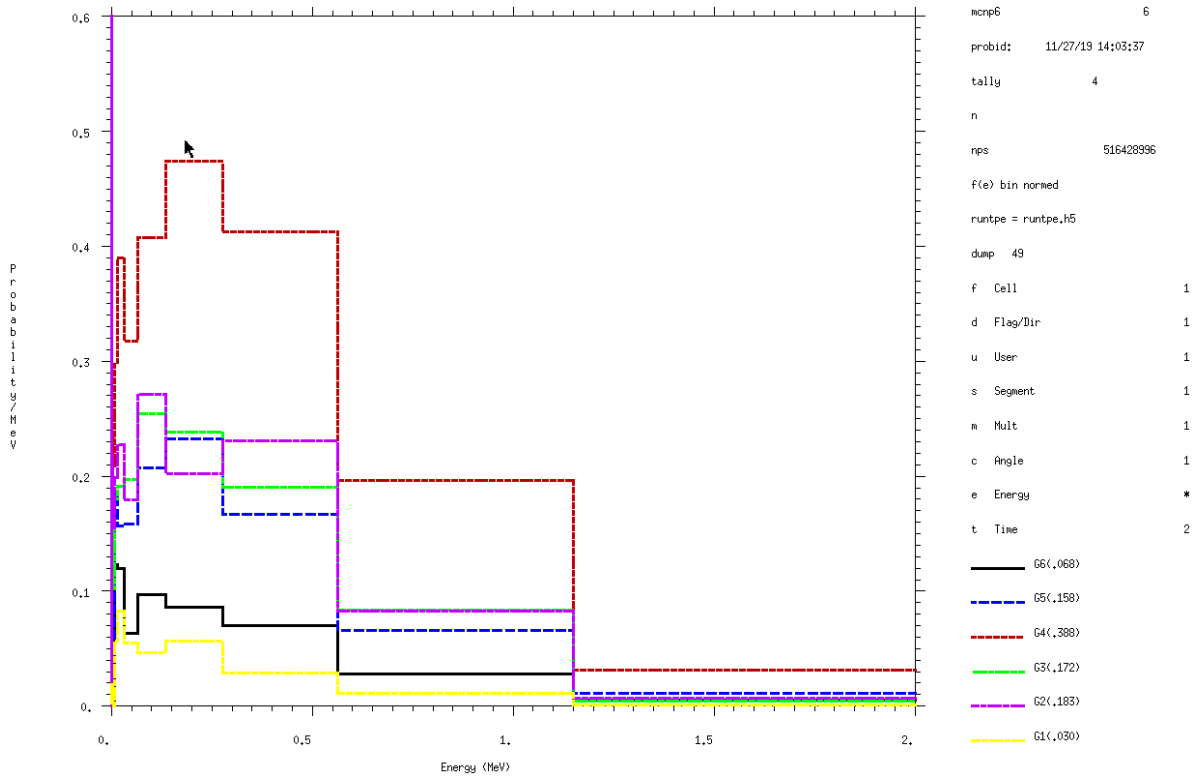


Figure 13. The delayed neutron spectra for the final 6 FNS time bins.

The spectral and integral values provided in Figs 12 and 13 are in good agreement with the published values for thermal fission of  $^{235}\text{U}$  (e.g.,  $\beta=0.0065$ , with the delayed relative yields provided in the label of the 2<sup>nd</sup> figure).

### 3 Verification against Nuclear Data Processing Codes

#### 3.1 Background

The objective is to verify the new MCNP multigroup (MG) tally feature works as expected when compared to MG cross sections produced by nuclear data processing codes, such as NJOY. In this work, the MCNP-computed MG cross sections are directly compared to those computed with NJOY2016 [1]. To ensure a meaningful comparison between these two methods, a proper weighting spectrum needs to be provided as input to NJOY. Figure 14 illustrates the approach taken in this verification effort to compare MCNP- and NJOY-computed MG cross sections, angular distributions, and energy spectra.

To achieve a consistent comparison between MCNP and NJOY, a single, ENDF/B-VIII.0 ENDF-6-formatted file for the  $^{239}\text{Pu}$  isotope is used as input to NJOY in both the first and third step in the process shown in Fig. 14. Another consistency requirement for the final NJOY calculation is the same weighting spectrum is needed. Within the MCNP calculation in the second step, the ultrafine

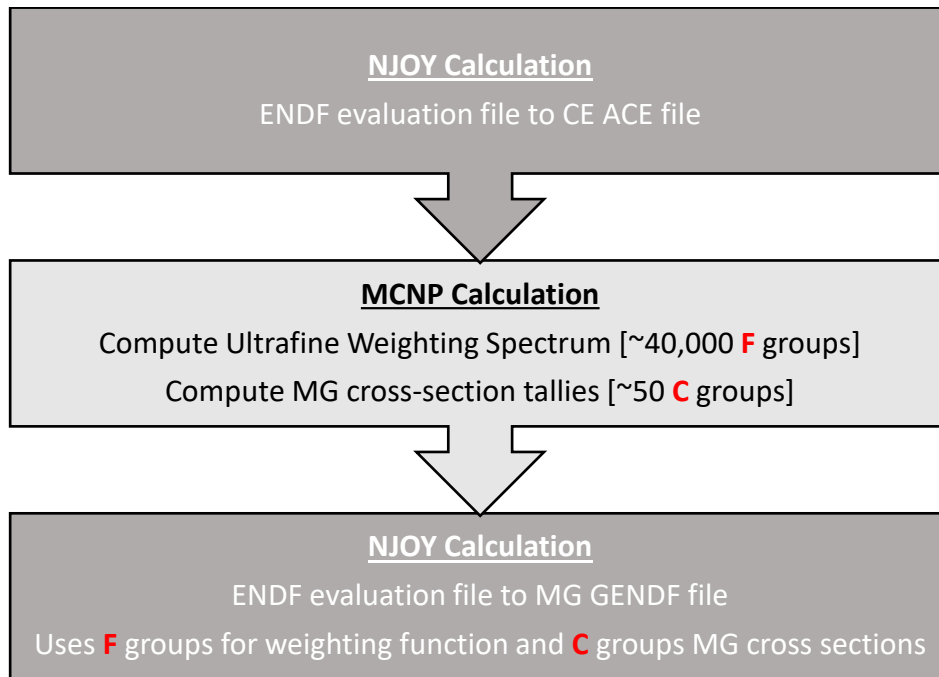


Figure 14. Calculation flow between NJOY and MCNP to compare multigroup cross sections, scattering angle distributions, and prompt/delayed fission spectra.

weighting spectrum is computed by tallying flux over the entire region of interest, binned in ~40,000 logarithmically-spaced energy bins. Given the number of tally bins required to compute this ultrafine weighting spectrum, a large number of particle histories are needed so the statistical uncertainties in the tally bins are sufficiently converged with valid confidence intervals.

The MCNP model test problem considered in this verification effort is a simple bare  $^{239}\text{Pu}$  sphere run in k-eigenvalue mode. In a bare metal configuration, the spectrum in the system is expected to be fast with little to no scattering down into the thermal neutron energy range. The full input file is provided in Appendix A.

An incomplete NJOY input file is provided in Appendix B. Given the size of the weighting spectrum computed by the MCNP F4 tally (~40,000 energy-flux pairs), the full listing of this spectrum is omitted. This NJOY input file serves to compute both the continuous-energy ACE-formatted file for MCNP, but also the resulting GENDF-formatted multigroup cross sections. Note the NJOY2016 source code was modified to allow for such a large user-provided weighting spectrum.

A simple and coarse multigroup energy-group structure was selected for the present work. This coarse energy-group structure consisted of 50 logarithmically spaced energy bins from  $10^{-11}$  to 20 MeV. In the MCNP input file in Appendix A, the coarse multigroup structure is defined in the E14, E24, E34 and E44 tally energy bin cards. In the NJOY input file in Appendix B, the same coarse multigroup structure is defined in the groupr module section of the input file.

### 3.2 Cross Section Verification

The 9 multigroup values, primarily consisting of cross sections, computed with the MCNP MGC special treatment tally option include inverse neutron velocity, total, capture, fission, absorption (capture + fission), scattering (total - absorption), prompt/total fission neutron production, delayed fission neutron production, and fission heating.

Figures 15-23 show the results of the direct comparison between the MCNP and NJOY computed multigroup cross sections for the aforementioned 9 multigroup cross sections. In each of the figures, the agreement is generally excellent with an average relative difference in MCNP and NJOY results between 1-8% and an average MCNP statistical uncertainty between 5-6% in the energy ranges above ~8 eV. Figure 24 shows the MCNP statistical uncertainties and discrepancies with the NJOY results corresponding to the MG total cross section values in Fig. 23. In the lower energies, where the statistical uncertainties in the MCNP calculation are significantly higher, the discrepancies are several factors or orders of magnitude smaller than the MCNP statistical uncertainties. The primary discrepancies appear at the resolved and unresolved resonance region transition energy ranges, with values ranging from a maximum discrepancy of 7-27% for cross section values in Figs. 16-23. These discrepancies can be resolved either through an optimally-designed energy group structure corresponding to the resolved/unresolved resonance energy transition point or through a finer weighting spectrum representation.

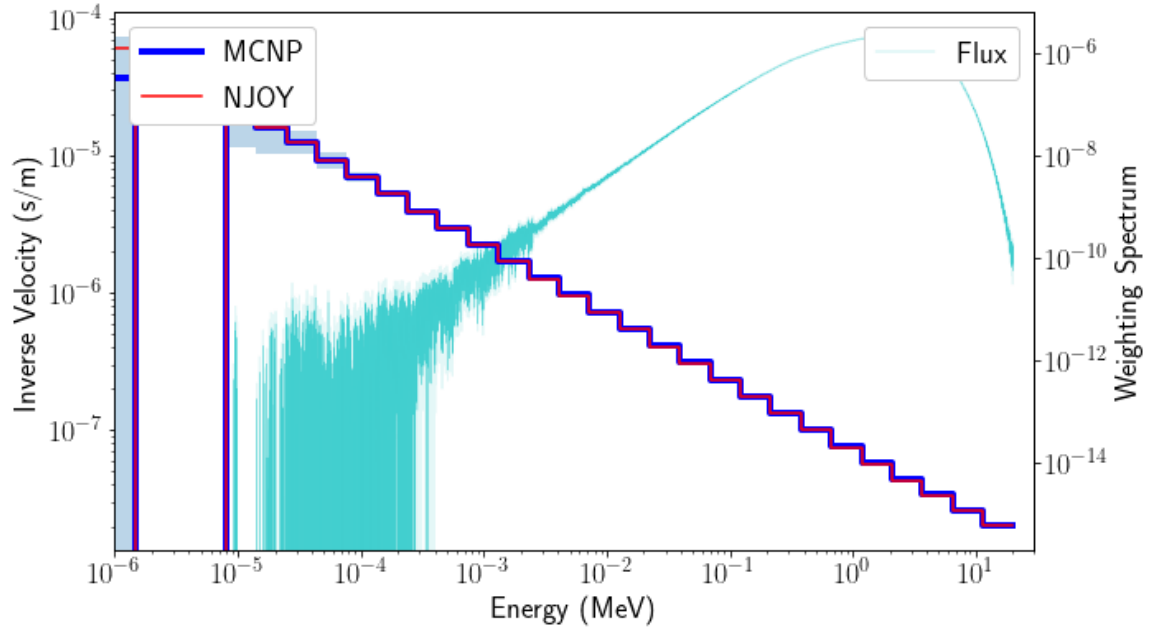


Figure 15. Neutron inverse velocity comparison. Light shaded blue indicates MCNP statistical uncertainties.

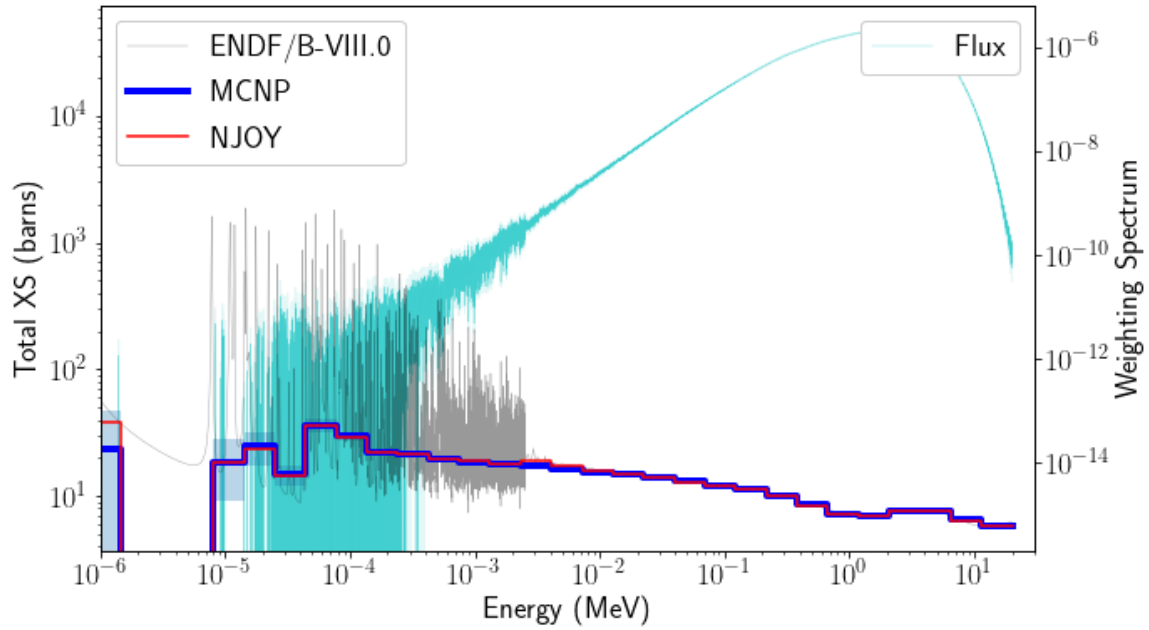


Figure 16. Total cross section comparison. Light shaded blue indicates MCNP statistical uncertainties.

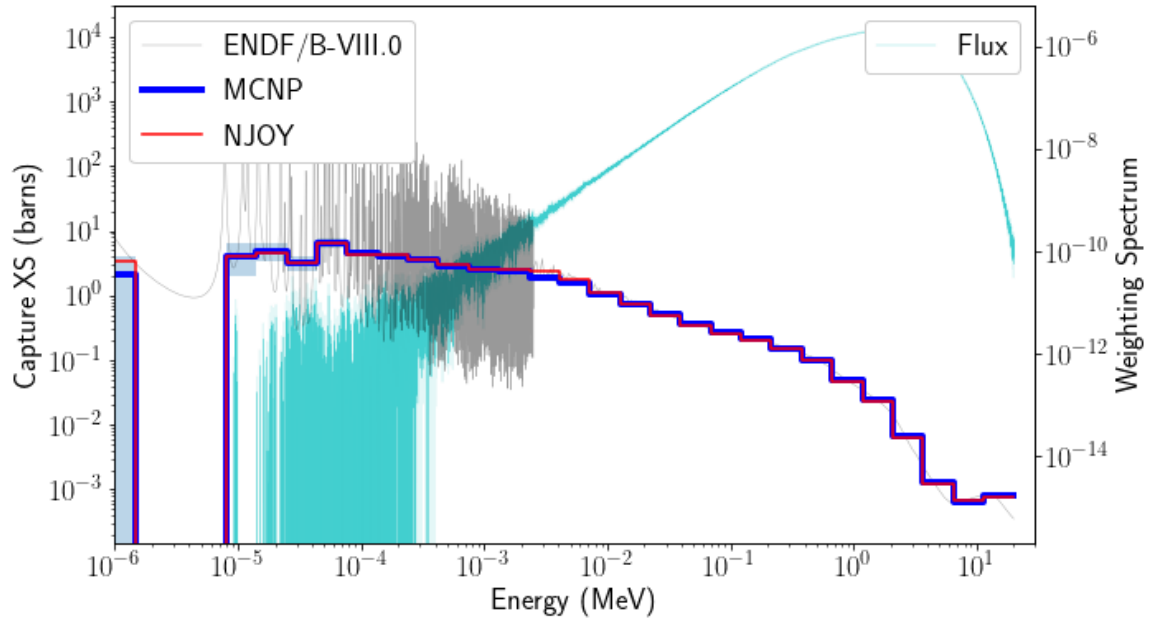


Figure 17. Capture cross section comparison. Light shaded blue indicates MCNP statistical uncertainties.

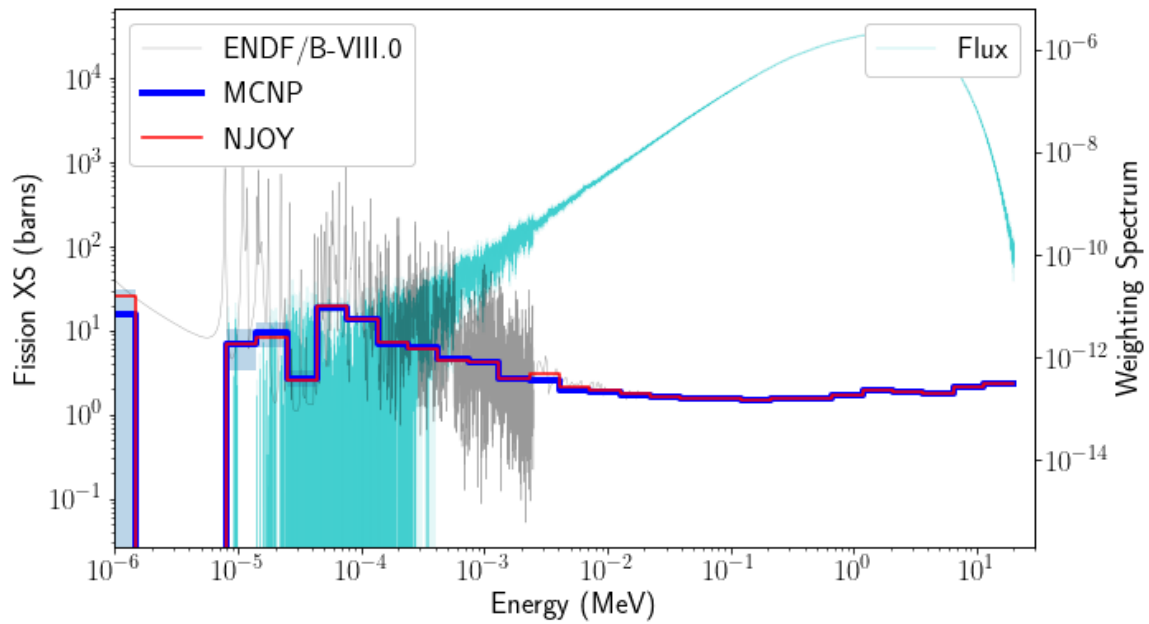


Figure 18. Fission cross section comparison. Light shaded blue indicates MCNP statistical uncertainties.

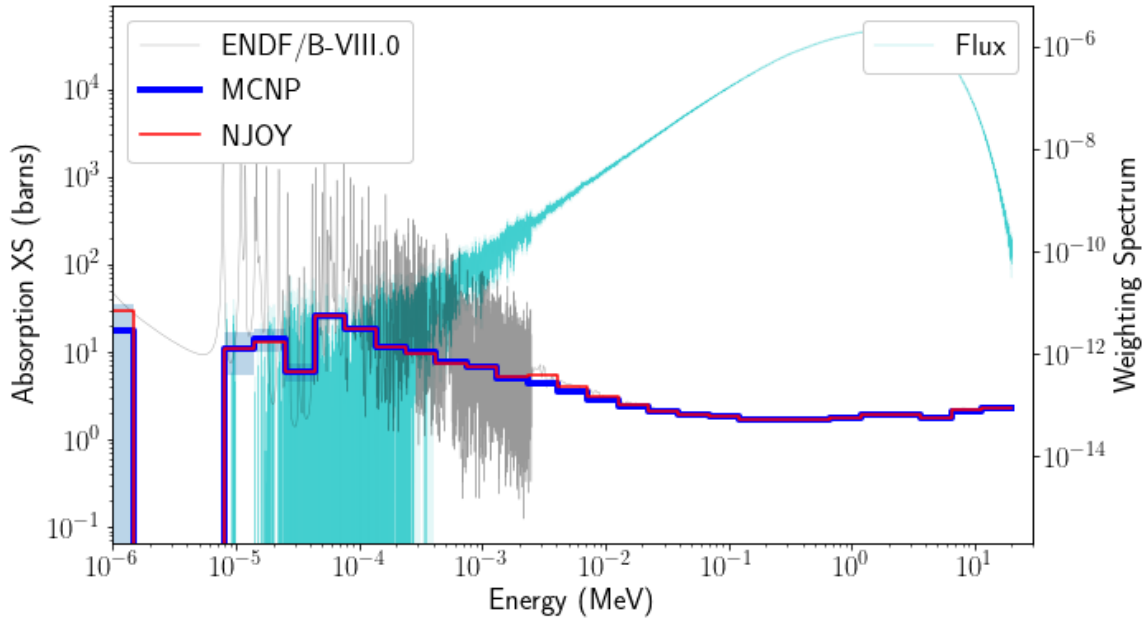


Figure 19. Absorption (capture + fission) cross section comparison.  
Light shaded blue indicates MCNP statistical uncertainties.

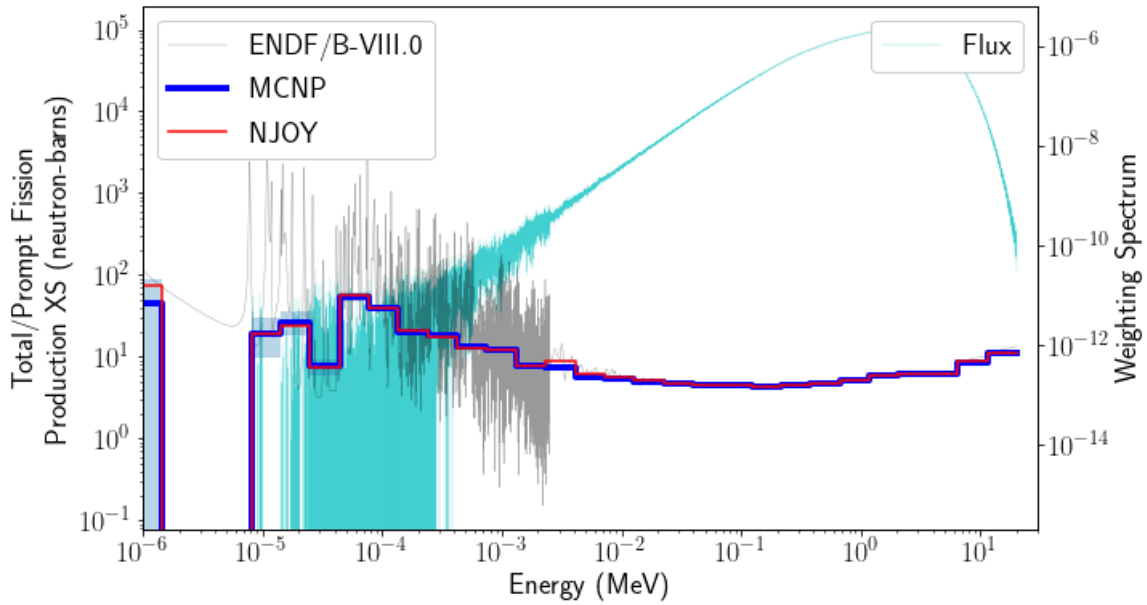


Figure 20. Total/prompt fission production cross section comparison.  
Light shaded blue indicates MCNP statistical uncertainties.

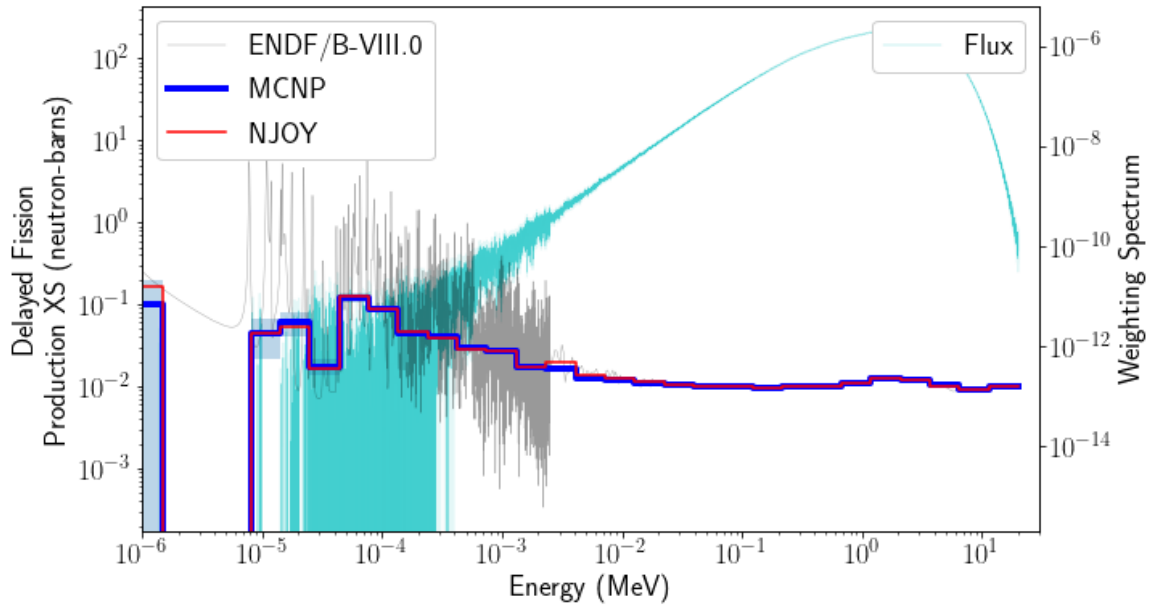


Figure 21. Delayed fission production cross section comparison.  
Light shaded blue indicates MCNP statistical uncertainties.

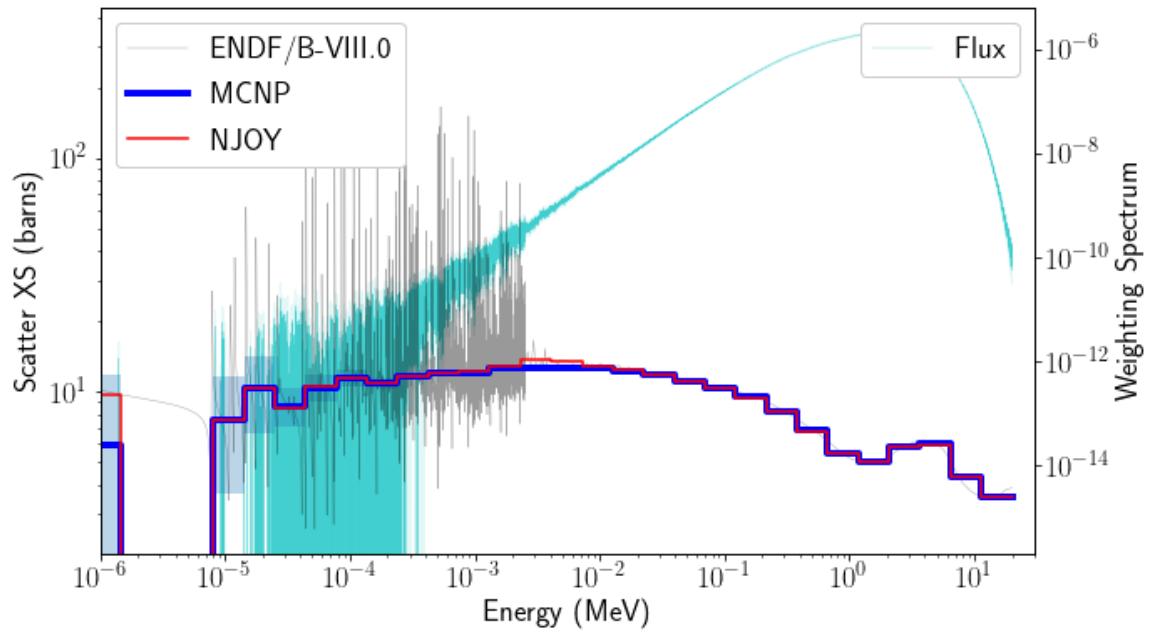


Figure 22. Scatter (total - absorption) cross section comparison.  
Light shaded blue indicates MCNP statistical uncertainties.

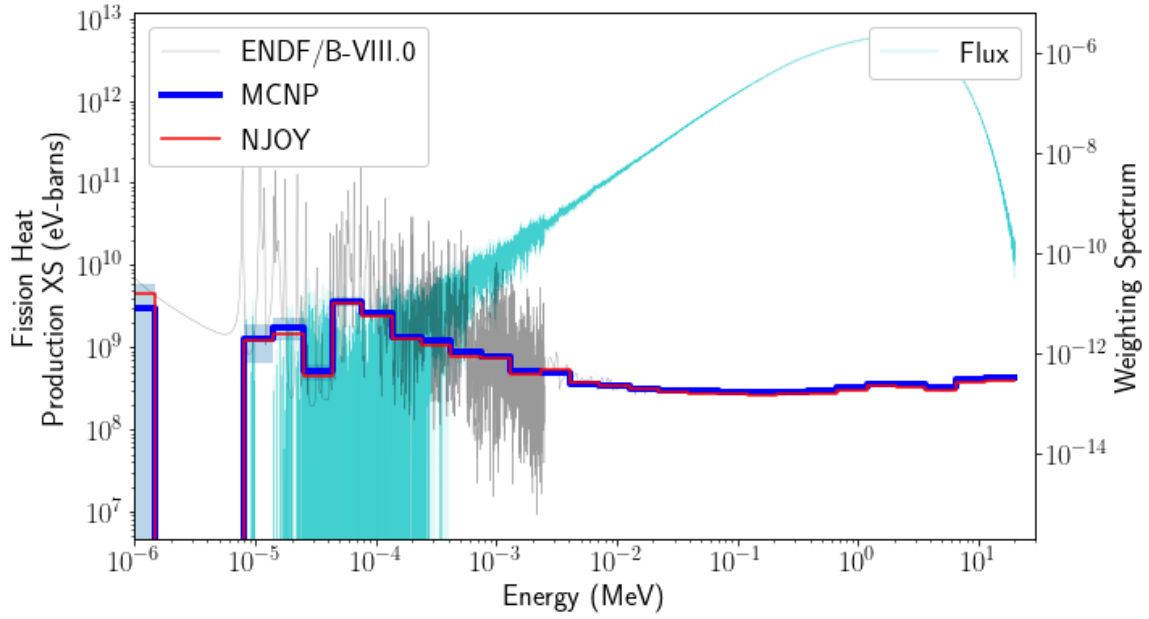


Figure 23. Fission heat production cross section comparison. Light shaded blue indicates MCNP statistical uncertainties.

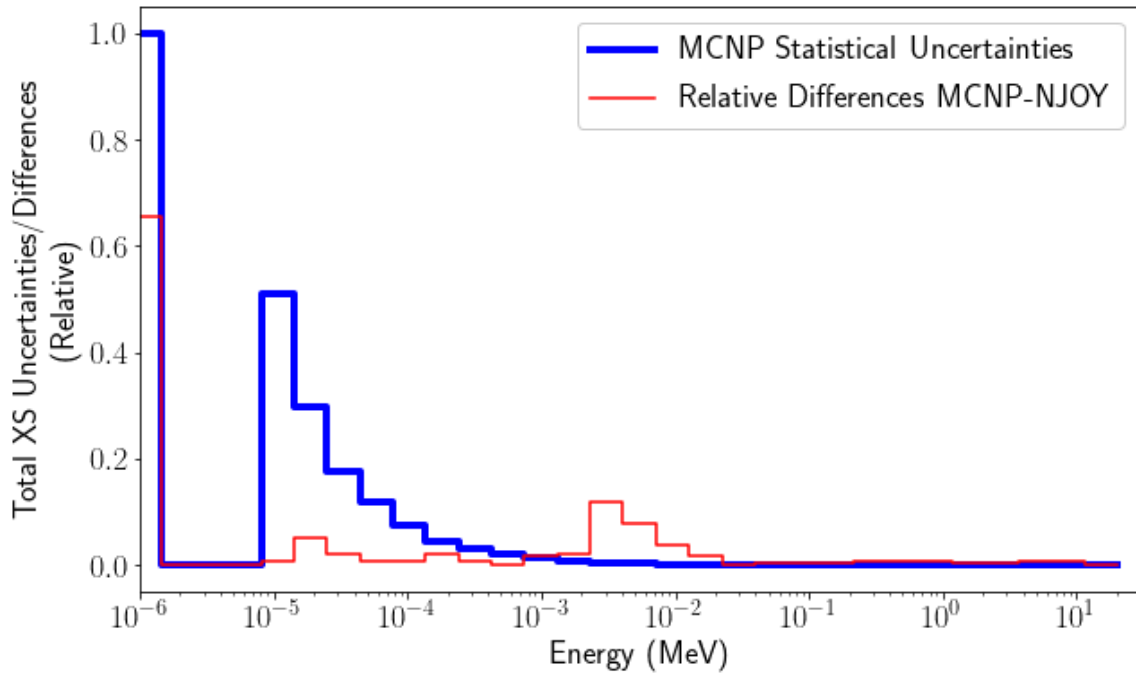


Figure 24. MCNP statistical uncertainties compared to discrepancies with the NJOY results for the total MG cross section.

### 3.3 Legendre coefficients for scattering verification

Given the two new MCNP scattering options, SPM and LCS, are consistent with one another, the LCS Legendre coefficients for scattering results were selected for this verification effort because these quantities are also produced by NJOY. Alternatively, the process described in Section 1.4 could be used to expand the NJOY-computed Legendre coefficients to compare to the MCNP-computed SPM quantities. In Fig. 25 the Legendre coefficients for incident group  $E_{g'}$  to outgoing group  $E_g$  scattering matrices are provided. Unlike standard NJOY and multigroup cross section conventions, the lower energies correspond to lower  $E_g$  group numbers and higher energies correspond to higher  $E_g$  group numbers.

The first column in Fig. 25 contains the NJOY results. In the second and third columns, the MCNP results are provided, including the statistical uncertainties of the MCNP mean values provided in the third column. The uncertainties in the lower off-diagonal elements of the scattering matrices are very large. Given these large uncertainties, the only reliable values in the MCNP results are those that correspond to the same dominant values in the NJOY results. The agreement in the results is as expected.

### 3.4 Fission Neutron Spectra verification

The fission neutron spectra, computed with the new MCNP FNS special treatment tally option, can be broken into a user-specified number of time bins, corresponding to the emission time of the neutrons born from fission. In this work, the prompt fission neutron spectrum and the default 6 delayed fission neutron groups in ENDF/B are computed and compared to the NJOY results.

In Figure 26, the prompt fission neutron spectrum matrix as a function of incident  $E_{g'}$  group and outgoing  $E_g$  group. The left and middle matrices from the NJOY and MCNP codes, respectively, are in excellent agreement where the MCNP statistical uncertainties, shown in the right matrix, are small. Like the Legendre scattering matrices, where the uncertainties in the MCNP results are large the mean values are unreliable and cannot not be reasonably compared to the NJOY results at the current level of statistical convergence.

The FNS option, through time-binning, computes the delayed fission neutron spectra matrices similar to the prompt fission neutron spectra matrix in Fig. 26. However, NJOY only produces the delayed fission neutron spectra independent of incident neutron energy. For the comparison of delayed fission neutron spectra in Fig. 27, the MCNP results are collapsed over all incident energies to obtain a single outgoing energy-dependent spectrum for each of the 6 groups.

Delayed fission groups 1 through 6 are ordered from shortest to longest half-life. The tally time bin boundaries, in shakes, for the delayed fission groups are  $10^2$ ,  $3.375 \times 10^7$ ,  $1.363 \times 10^8$ ,  $4.115 \times 10^8$ ,  $1.392 \times 10^9$ ,  $3.8175 \times 10^9$ ,  $1.6353 \times 10^{10}$ . As noted in Section 1.5, these values correspond to the midpoints for published  $^{235}\text{U}$  half-life values. Note that while the results appear to be consistent between MCNP and NJOY in Fig. 27, there is an inconsistency between the plotted values. NJOY values are coming from each individual delayed fission group. MCNP values are coming from these time bin boundaries used to nominally separate the delayed fission groups.

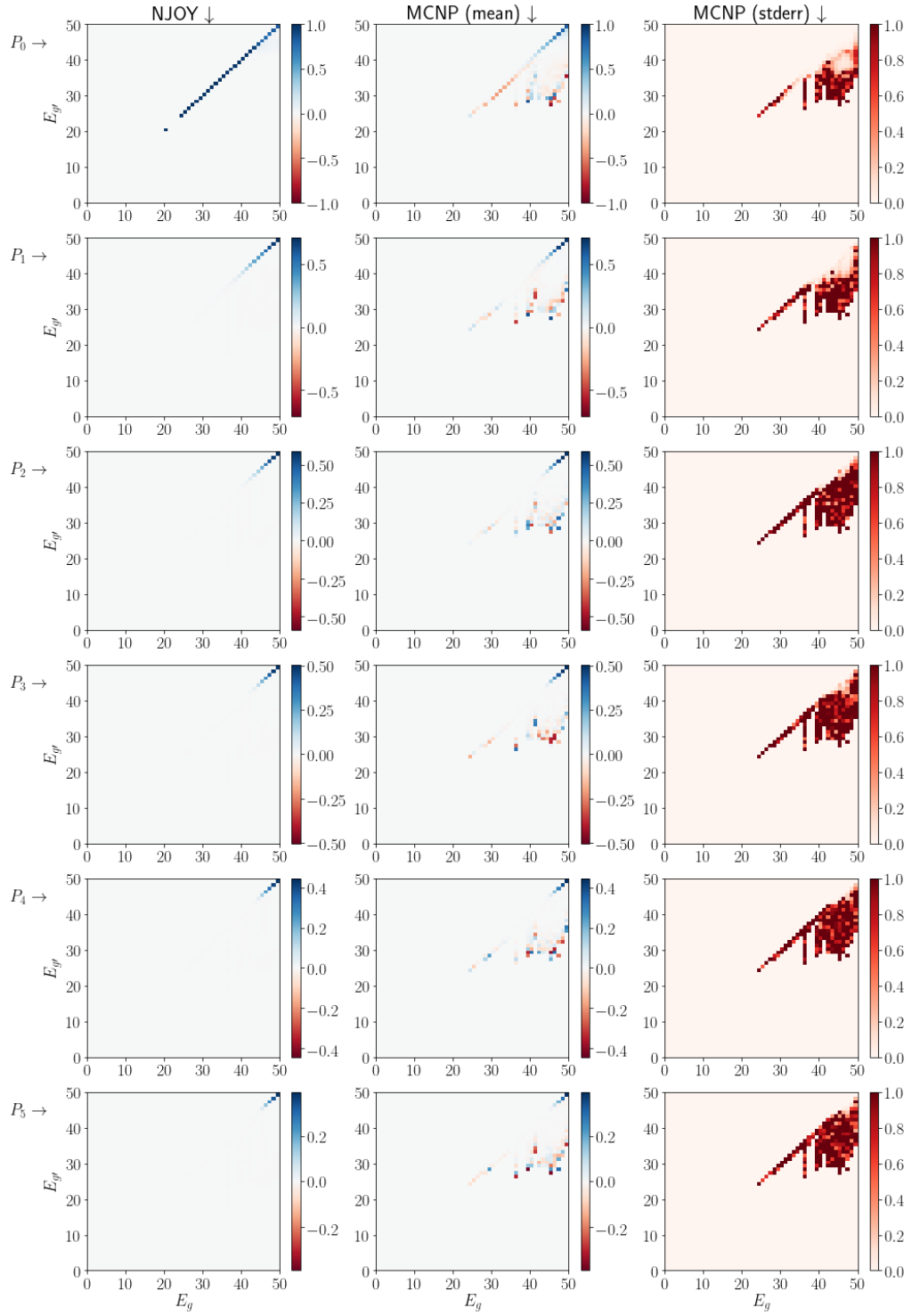


Figure 25. Legendre coefficients for scattering from incident energy group  $E_g$  to outgoing energy group  $E_g$ .

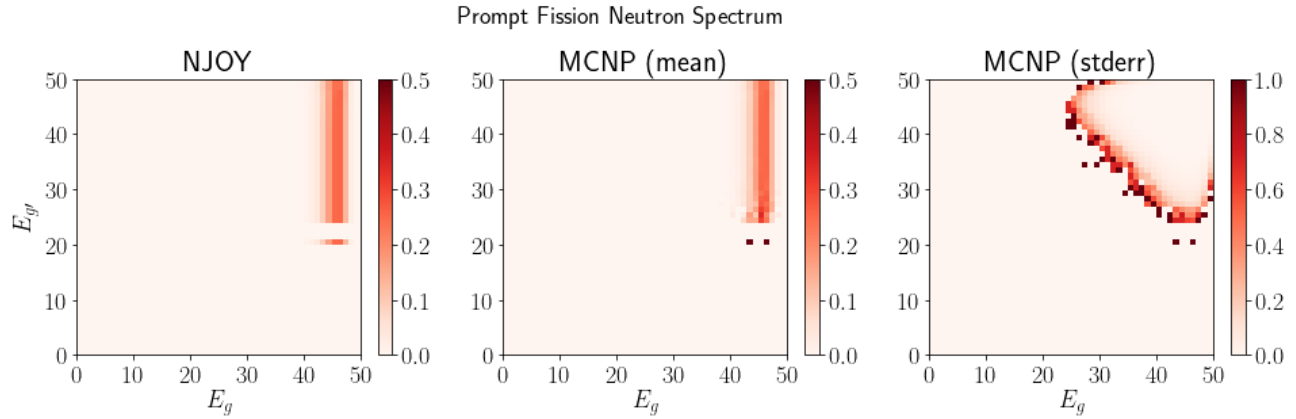


Figure 26. Prompt fission neutron spectrum from incident energy group  $E_g$  to outgoing energy group  $E_g'$ .

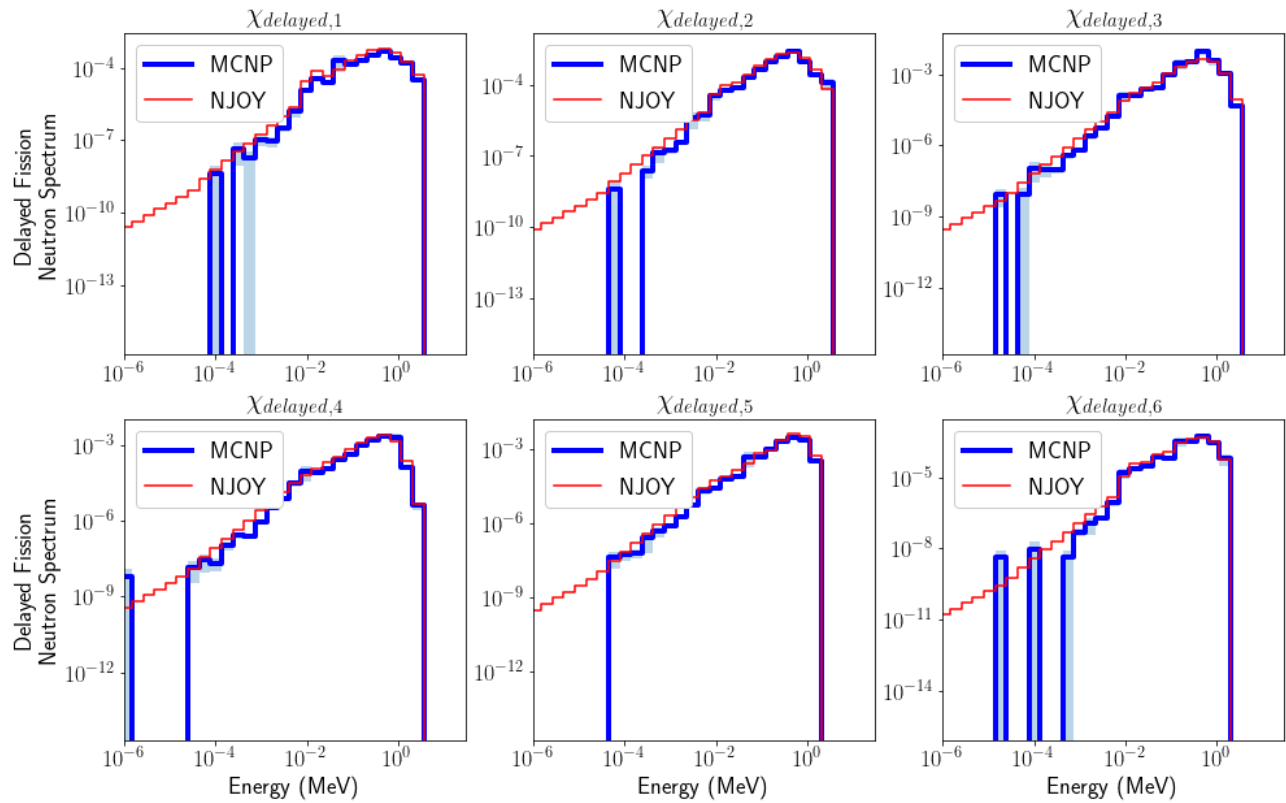


Figure 27. Delayed fission neutron spectra for the 6 ENDF/B delayed fission groups. Light shaded blue indicates MCNP statistical uncertainties.

### 3.5 Summary of MCNP-NJOY Comparisons

The comparison between the NJOY- and MCNP-computed multigroup cross sections are generally in excellent agreement. While a large number of histories ( $10^9$ ) in the MCNP calculation were used in computing the multigroup cross sections, large statistical uncertainties can persist that make the

comparison more challenging. It will be important in future work to investigate variance reduction techniques as they apply to multigroup cross-section tallies.

### 3.6 MCNP-OpenMC Reactor Comparison

The tallies discussed here were then applied to a simple reactor geometry to analyze the resulting cross sections. The MCNP multigroup tallies were compared to equivalent cross section results in the OpenMC [1] radiation transport tool. As an open source code, OpenMC is readily available to compare codes for neutron transport making it a good test subject for reasonable results from MCNP. To make equivalent models, the same continuous energy cross sections are provided to both MCNP and OpenMC. Equivalent geometries and cross sections in both tools should provide excellent agreement between the tools within statistical uncertainty.

This tool was initially funded to implement cross sections generation for reactor applications. To confirm accuracy of solution, a simple reactor geometry was modeled in each tool and then tallied for comparison results. The fuel rods consist of tristructural-isotopic (TRISO) fuel with small kernels of uranium of 19.75% enrichment surrounded by SiC and C layers within a graphite matrix. Moderating material exists both in the form of the graphite structural monolith that contains the fuel rods and heat pipes, plus additional yttrium hydride rods to slow neutrons down and reduce the necessary fuel mass. Figure 28 shows a unit cell model of the Snowflake design, which for the code comparison is infinitely reflecting on all sides. The TRISO fuel in green will be the direct comparison of cross sections discussed here. Fuel provides each cross section tally including fission cross sections and fission neutron spectra which shows the comparison of each tally generated for MCNP including MGC, LCS, and FNS. The SPM tally is very similar to LCS except for discrete cosine binning to account for anisotropic factors. The cross sections were both tallied around room temperature (300K) for the model comparison.

In total, three tallies are highlighted here for comparison including multigroup cross sections (MGC), scattering coefficients matrix (LCS), and fission neutron spectra (FNS). The SPM tally is not compared here as the geometry will not implement discrete cosine angles in deterministic

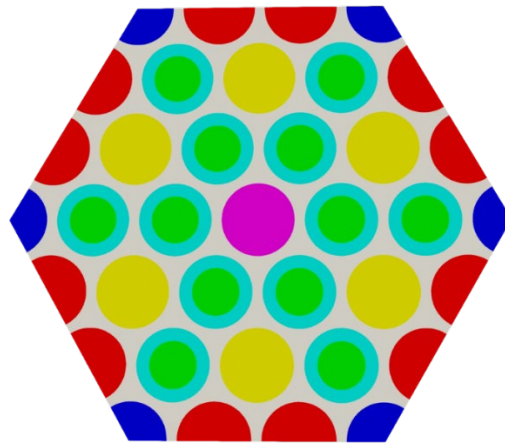


*Figure 28: Snowflake assembly model for cross section comparison. Yttrium hydride is in Red, sodium heat pipes are modeled in three separate rows of Blue, Yellow, and Pink, and TRISO fuel is shown as Green with a surrounding layer of graphite in turquoise. A light gray monolith of graphite is also interjoining the pieces.*

transport. Also, OpenMC was run for Legendre coefficient scattering results only. The first tally highlights the results from the MGC tally option followed by the LCS and FNS comparisons. Multiple cross sections are compared here in Tables 1 - 4 for total, fission, kappa-fission, and neutron velocity. These highlight the comparisons where similarities and methodology differences occur. A 20-group structure was implemented to capture the full-spectrum of neutrons with a particular focus on the thermal region. For reference, the group bin selections are seen in each MGC table (Table 1 - 4). The minimum energy for tallying was 0.0 MeV to capture low energy neutrons.

### 3.7 The Multigroup Cross Section (MGC) Tally Comparison

The total macroscopic cross sections show excellent agreement with less than 2% difference between the two tools. The results are shown in Table 2. The thermal group exhibits the largest difference where most other cross sections were less than 0.5%. It's unclear why the thermal group has different cross sections. Transport could default to different methodologies for handling lower-energy neutrons. Based on higher cross section from OpenMC, a more thermalized spectrum is likely seen in the fuel region. There is also a spike in variation for the 4.00E-6 - 9.88E-6 MeV bin. This location directly correlates to the first U238 resonance and multiple U235 resonances thus is more likely a resonance methodology handling within the transport tool. The variation is still less than 1% between the two tools which indicates adequate implementation in MCNP.

The fission cross sections also show good overall agreement. The largest difference resides in the resonance energy bin discussed for the total cross sections. The variation is almost 4% between the two tools. A slight spectrum shift from both U235 and U238 resonances could be adjusting these results as well but have a more direct impact on the fission cross section. Most remaining cross sections are nearly identical between the two different tools. Again, this variation is likely due to varying methodologies for handling resonances between the two tools.

The third cross section directly compared here is the kappa-fission cross section which multiplies the fission cross section by the kappa heating factor. The results, as shown in Table 3, note significant differences in kappa-fission results. With equivalent kappa values, the results should display equal variation to the fission cross sections. The kappa-fission values were then divided by the fission cross section to see where the kappa values differ. Based on the results in Table 4, the kappa values are calculated differently between each transport tool. OpenMC produces between 193-197 MeV which suggests only neutrinos are not deposited locally. MCNP values are around 181 MeV in all energy groups. These results suggest a removal of certain delayed particles as well as neutrinos. These methodology differences explain the variation between each tool. In deterministic transport tools, the main impact from these results would be the calculated fission rate to produce a certain power level. MCNP would produce higher burnups of fuel to accomplish the same power level. Overall, the tallies displayed do show good agreement between MCNP and OpenMC for equivalent tallies. The user should be aware of the differing methodologies shown here.

The final tally looks at the neutron velocities in each bin. The results are shown in Table 5. These results are quite informative to understand what flux was seen in each group. Based on the results, OpenMC's thermal group has a harder spectrum than MCNP. This result does not support the

assertion of a more thermalized flux in the fuel for OpenMC to have higher cross sections. Statistical uncertainty may give a more reasonable explanation for the discrepancies seen.

Table 2: TRISO Fuel Total Cross Section Comparison. Good agreement between both tools in all groups. Small variation in the thermal group.

<b>Total Cross Section</b>					
<b>Max Energy Bin Edge (MeV)</b>	<b>OpenMC</b>	<b>OpenMC Error</b>	<b>MCNP</b>	<b>MCNP Error</b>	<b>% Difference</b>
5.80E-8	4.56E-01	7.86E-05	4.47E-01	0.0001	1.99
1.40E-7	3.80E-01	7.22E-05	3.78E-01	0.0001	0.69
3.50E-7	3.56E-01	7.02E-05	3.55E-01	0.0001	0.35
6.25E-7	3.30E-01	9.33E-05	3.30E-01	0.0002	0.18
1.02E-6	3.20E-01	9.04E-05	3.20E-01	0.0002	0.12
1.86E-6	3.16E-01	8.05E-05	3.16E-01	0.0002	0.05
4.00E-6	3.11E-01	6.81E-05	3.11E-01	0.0001	0.01
9.88E-6	3.96E-01	9.17E-05	4.00E-01	0.0001	0.98
1.60E-5	3.20E-01	8.62E-05	3.20E-01	0.0001	0.01
1.49E-4	3.80E-01	5.78E-05	3.80E-01	0.0001	0.01
5.53E-3	3.42E-01	3.69E-05	3.42E-01	0.0001	0.01
9.12E-3	3.26E-01	8.69E-05	3.26E-01	0.0001	0.01
1.11E-1	3.11E-01	3.67E-05	3.11E-01	0.0001	0.01
5.00E-1	2.84E-01	2.79E-05	2.84E-01	0.0001	0.01
8.21E-1	2.23E-01	3.61E-05	2.23E-01	0.0001	0.01
1.35E0	1.92E-01	3.02E-05	1.92E-01	0.0001	0.01
2.23E0	1.51E-01	2.40E-05	1.51E-01	0.0001	0.01
3.68E0	1.45E-01	3.49E-05	1.45E-01	0.0001	0.01
6.07E0	1.35E-01	5.03E-05	1.35E-01	0.0002	0.02
2.00E1	1.01E-01	8.79E-05	1.01E-01	0.0004	0.01

### 3.7 Legendre Coefficient Scattering (LCS) Tally Comparison

The second tally looks at the scattering coefficients in the tool. Comparison plots are difficult to convey with 20 groups, but 20x20 groups were plotted in Tables 6-9. These results are for isotropic scattering coefficients only. Further Legendre coefficients to high order are not plotted here though both tools are capable of generating high order scattering. Tables 6-9 show MCNP and OpenMC results and their respective differences. The scattering tallies are typically difficult to tally well in each tool due to statistics, but the results are generally close between each tool. The percent difference in Table 9 ignores very low scattering probability ( $<1.0E-5$ ) regions because these can result in huge percent variations. Those results are tallied but set to 0.0 here. Most in-group

Table 3: TRISO Fuel Fission Cross Section Comparison. MCNP is slightly higher in most cross sections.

<b>Fission Cross Section</b>					
<b>Max Energy Bin Edge (MeV)</b>	<b>OpenMC</b>	<b>OpenMC Error</b>	<b>MCNP</b>	<b>MCNP Error</b>	<b>% Difference</b>
5.80E-8	1.10E-01	1.92E-05	1.12E-01	0.0001	1.47
1.40E-7	5.67E-02	1.08E-05	5.72E-02	0.0001	0.82
3.50E-7	3.76E-02	7.43E-06	3.77E-02	0.0001	0.28
6.25E-7	1.93E-02	5.48E-06	1.93E-02	0.0002	0.05
1.02E-6	1.17E-02	3.31E-06	1.17E-02	0.0002	0.01
1.86E-6	7.80E-03	2.17E-06	7.72E-03	0.0002	0.93
4.00E-6	3.92E-03	9.61E-07	3.99E-03	0.0002	1.87
9.88E-6	8.23E-03	2.88E-06	8.56E-03	0.0002	4.03
1.60E-5	7.74E-03	2.71E-06	7.75E-03	0.0002	0.01
1.49E-4	7.46E-03	1.42E-06	7.46E-03	0.0001	0.00
5.53E-3	2.11E-03	2.66E-07	2.11E-03	0.0001	0.03
9.12E-3	6.59E-04	1.76E-07	6.59E-04	0.0001	0.02
1.11E-1	4.13E-04	4.96E-08	4.13E-04	0.0001	0.01
5.00E-1	2.59E-04	2.54E-08	2.59E-04	0.0001	0.01
8.21E-1	2.34E-04	3.77E-08	2.34E-04	0.0001	0.01
1.35E0	3.48E-04	5.58E-08	3.48E-04	0.0001	0.01
2.23E0	1.70E-03	2.81E-07	1.70E-03	0.0001	0.01
3.68E0	2.05E-03	4.95E-07	2.05E-03	0.0001	0.01
6.07E0	2.08E-03	7.75E-07	2.08E-03	0.0002	0.01
2.00E1	3.27E-03	2.88E-06	3.27E-03	0.0005	0.01

Table 4: Kappa-Fission Cross Section Comparison. MCNP is consistently lower due to lower kappa values. MCNP is removing several decay power fractions whereas OpenMC maintains all but neutrinos.

<b>Kappa-Fission Cross Section</b>				
<b>Max Energy Bin Edge (MeV)</b>	<b>OpenMC</b>	<b>MCNP</b>	<b>OpenMC Kappa (eV/fission)</b>	<b>MCNP Kappa (eV/fission)</b>
5.80E-8	2.14E+07	2.03E+07	1.93E+08	1.809E+08
1.40E-7	1.10E+07	1.03E+07	1.93E+08	1.809E+08
3.50E-7	7.27E+06	6.82E+06	1.93E+08	1.809E+08
6.25E-7	3.73E+06	3.49E+06	1.93E+08	1.809E+08
1.02E-6	2.27E+06	2.12E+06	1.93E+08	1.809E+08
1.86E-6	1.51E+06	1.40E+06	1.93E+08	1.809E+08
4.00E-6	7.58E+05	7.22E+05	1.93E+08	1.809E+08
9.88E-6	1.59E+06	1.55E+06	1.93E+08	1.809E+08
1.60E-5	1.50E+06	1.40E+06	1.93E+08	1.809E+08
1.49E-4	1.44E+06	1.35E+06	1.93E+08	1.809E+08
5.53E-3	4.08E+05	3.82E+05	1.93E+08	1.809E+08
9.12E-3	1.28E+05	1.19E+05	1.93E+08	1.809E+08
1.11E-1	7.99E+04	7.47E+04	1.93E+08	1.809E+08
5.00E-1	5.00E+04	4.68E+04	1.93E+08	1.809E+08
8.21E-1	4.52E+04	4.22E+04	1.93E+08	1.809E+08
1.35E0	6.78E+04	6.30E+04	1.95E+08	1.810E+08
2.23E0	3.35E+05	3.08E+05	1.97E+08	1.812E+08
3.68E0	4.04E+05	3.71E+05	1.97E+08	1.813E+08
6.07E0	4.10E+05	3.77E+05	1.97E+08	1.813E+08
2.00E1	6.46E+05	5.93E+05	1.97E+08	1.813E+08

Table 5: Neutron Velocity Comparison

<b>Neutron Velocities</b>			
<b>Max Energy Bin Edge (MeV)</b>	<b>OpenMC (cm/s)</b>	<b>MCNP (cm/s)</b>	<b>% Difference</b>
5.80E-8	2.29E+05	2.263E+05	1.35
1.40E-7	4.05E+05	4.024E+05	0.66
3.50E-7	6.25E+05	6.173E+05	1.25
6.25E-7	9.41E+05	9.408E+05	0.01
1.02E-6	1.23E+06	1.232E+06	0.04
1.86E-6	1.62E+06	1.618E+06	0.13
4.00E-6	2.26E+06	2.284E+06	0.82
9.88E-6	3.44E+06	3.474E+06	0.86
1.60E-5	4.89E+06	4.887E+06	0.00
1.49E-4	9.30E+06	9.297E+06	0.00
5.53E-3	3.69E+07	3.693E+07	0.01
9.12E-3	1.16E+08	1.163E+08	0.00
1.11E-1	2.43E+08	2.429E+08	0.00
5.00E-1	6.78E+08	6.783E+08	0.02
8.21E-1	1.11E+09	1.107E+09	0.05
1.35E0	1.42E+09	1.418E+09	0.08
2.23E0	1.81E+09	1.809E+09	0.14
3.68E0	2.29E+09	2.284E+09	0.22
6.07E0	2.94E+09	2.932E+09	0.36
2.00E1	3.72E+09	3.699E+09	0.58

scattering results show good agreement between both tools. The percent variation shown in Table 9 is less than 3% between MCNP and OpenMC. Which again is in the thermal group which as suggested in the cross section discussion, the methods may employ different methods causing a shift in thermal flux in the fuel. The out-group scattering shows good agreement between the tools. Some upscatter and downscatter cross sections have notable differences up to 17% which is likely more the just (n,xn) scattering effects. It's difficult to establish why this behavior is occurring though resonances may still play a role. Another option for the scattering tallies is the lower probabilities of upscatter and some downscatter events. To reduce the statistical uncertainty, a very long run in both MCNP and OpenMC would be required to accomplish such a task. For the purposes of validation, these results indicate correct behavior for the vast majority of the results and the methodology is being performed correctly with slight variations in the transport method or statistical uncertainty.

Table 6: MCNP Scattering Coefficient Matrix. Multiplicity matrix multiplied by scattering coefficients.

2.7E-01	3.7E-02	7.7E-05	0.0E+00																
5.7E-02	2.4E-01	1.1E-02	1.5E-08	0.0E+00															
7.5E-04	6.4E-02	2.4E-01	3.1E-03	8.9E-09	0.0E+00														
1.2E-08	4.3E-05	7.1E-02	2.3E-01	3.0E-03	0.0E+00														
0.0E+00	0.0E+00	4.0E-04	8.3E-02	2.2E-01	1.6E-03	0.0E+00													
0.0E+00	0.0E+00	0.0E+00	4.0E-04	6.7E-02	2.4E-01	4.9E-04	0.0E+00												
0.0E+00	0.0E+00	0.0E+00	0.0E+00	4.7E-06	5.0E-02	2.5E-01	1.2E-04	0.0E+00											
0.0E+00	0.0E+00	0.0E+00	0.0E+00	0.0E+00	0.0E+00	4.2E-02	2.7E-01	2.4E-05	0.0E+00										
0.0E+00	8.8E-02	2.1E-01	0.0E+00																
0.0E+00	1.8E-02	3.2E-01	0.0E+00																
0.0E+00	1.1E-02	3.2E-01	0.0E+00																
0.0E+00	8.3E-02	2.4E-01	0.0E+00																
0.0E+00	1.1E-08	7.2E-06	1.4E-02	3.0E-01	0.0E+00	0.0E+00	0.0E+00	0.0E+00	0.0E+00	0.0E+00									
0.0E+00	1.0E-07	1.7E-07	2.0E-02	2.6E-01	0.0E+00	0.0E+00	0.0E+00	0.0E+00	0.0E+00										
0.0E+00	1.1E-06	1.7E-06	2.1E-04	5.6E-02	1.7E-01	0.0E+00	0.0E+00	0.0E+00	0.0E+00										
0.0E+00	1.4E-08	2.4E-06	3.7E-06	5.1E-04	3.1E-03	4.8E-02	1.4E-01	0.0E+00	0.0E+00										
0.0E+00	0.0E+00	0.0E+00	0.0E+00	0.0E+00	0.0E+00	2.0E-09	0.0E+00	2.0E-09	0.0E+00	5.0E-08	8.9E-06	1.0E-05	4.7E-04	3.9E-03	2.7E-03	3.9E-02	1.0E-01	0.0E+00	0.0E+00
0.0E+00	2.3E-08	1.3E-06	1.7E-06	2.6E-04	3.2E-03	2.9E-03	3.3E-03	4.2E-02	9.1E-02	0.0E+00									
0.0E+00	7.0E-09	0.0E+00	1.3E-06	1.5E-06	2.3E-04	2.6E-03	2.5E-03	2.7E-03	2.6E-03	3.7E-02	8.5E-02								
0.0E+00	5.0E-06	4.2E-06	3.3E-04	2.3E-03	1.9E-03	4.6E-03	7.4E-03	4.8E-03	2.4E-02										

Table 7: Nu-Scatter OpenMC Matrix. Slight adjustment for (n,xn) reactions in OpenMC.

2.8E-01	4.0E-02	8.1E-05	0.0E+00																
5.5E-02	2.4E-01	1.3E-02	1.1E-08	0.0E+00															
6.7E-04	5.8E-02	2.4E-01	3.5E-03	6.0E-09	0.0E+00														
3.3E-19	4.3E-05	7.1E-02	2.3E-01	3.0E-03	0.0E+00														
0.0E+00	0.0E+00	4.1E-04	8.3E-02	2.2E-01	1.6E-03	0.0E+00													
1.7E-19	0.0E+00	0.0E+00	4.1E-04	6.8E-02	2.4E-01	4.7E-04	0.0E+00												
0.0E+00	0.0E+00	0.0E+00	0.0E+00	5.1E-06	5.5E-02	2.5E-01	1.0E-04	0.0E+00											
0.0E+00	0.0E+00	2.1E-18	0.0E+00	0.0E+00	0.0E+00	4.8E-02	2.6E-01	2.3E-05	0.0E+00										
0.0E+00	8.8E-02	2.1E-01	0.0E+00																
0.0E+00	1.8E-02	3.2E-01	0.0E+00																
0.0E+00	1.1E-02	3.2E-01	0.0E+00																
0.0E+00	8.3E-02	2.4E-01	0.0E+00																
0.0E+00	4.6E-09	7.3E-06	1.4E-02	3.0E-01	0.0E+00														
0.0E+00	1.1E-07	1.8E-07	2.0E-02	2.6E-01	0.0E+00	0.0E+00	0.0E+00	0.0E+00	0.0E+00	0.0E+00									
0.0E+00	9.3E-07	1.7E-06	2.1E-04	5.6E-02	1.7E-01	0.0E+00	0.0E+00	0.0E+00	0.0E+00	0.0E+00									
0.0E+00	4.1E-09	1.2E-08	2.6E-06	3.7E-06	5.1E-04	3.1E-03	4.8E-02	1.4E-01	0.0E+00	0.0E+00	0.0E+00	0.0E+00							
0.0E+00	3.7E-08	8.8E-06	9.9E-06	4.7E-04	3.9E-03	2.7E-03	3.9E-02	1.0E-01	0.0E+00	0.0E+00	0.0E+00								
0.0E+00	2.0E-08	1.5E-06	1.8E-06	2.6E-04	3.2E-03	2.9E-03	3.3E-03	4.2E-02	9.1E-02	0.0E+00	0.0E+00								
0.0E+00	1.5E-06	1.7E-06	2.4E-04	2.6E-03	2.5E-03	2.7E-03	2.6E-03	3.7E-02	8.5E-02	0.0E+00									
0.0E+00	1.3E-07	5.5E-06	4.1E-06	3.3E-04	2.4E-03	1.9E-03	4.7E-03	7.5E-03	4.9E-03	2.4E-02	4.9E-02								

Table 8: MCNP - OpenMC absolute difference in scattering cross section.

9.0E-03	2.2E-03	4.2E-06	0.0E+00																
1.7E-03	3.5E-03	1.4E-03	4.4E-09	0.0E+00															
8.2E-05	5.2E-03	6.2E-03	4.0E-04	2.9E-09	0.0E+00														
1.2E-08	6.5E-07	1.0E-04	7.5E-04	4.0E-05	0.0E+00														
0.0E+00	0.0E+00	5.7E-06	4.7E-04	3.7E-05	3.6E-05	0.0E+00													
1.7E-19	0.0E+00	0.0E+00	6.6E-06	1.1E-03	1.0E-03	1.6E-05	0.0E+00												
0.0E+00	0.0E+00	0.0E+00	0.0E+00	3.4E-07	4.3E-03	4.2E-03	1.7E-05	0.0E+00											
0.0E+00	0.0E+00	2.1E-18	0.0E+00	0.0E+00	0.0E+00	6.1E-03	6.3E-03	8.2E-07	0.0E+00										
0.0E+00	3.4E-05	5.6E-05	0.0E+00																
0.0E+00	6.8E-06	4.0E-05	0.0E+00																
0.0E+00	3.0E-06	3.2E-05	0.0E+00																
0.0E+00	3.4E-05	4.1E-06	0.0E+00																
0.0E+00	6.6E-09	1.7E-07	8.8E-06	4.2E-05	0.0E+00														
0.0E+00	9.8E-09	7.5E-09	2.7E-06	2.6E-05	0.0E+00	0.0E+00	0.0E+00	0.0E+00	0.0E+00	0.0E+00									
0.0E+00	1.4E-07	8.6E-09	2.9E-06	1.4E-05	3.7E-05	0.0E+00	0.0E+00	0.0E+00	0.0E+00	0.0E+00									
0.0E+00	4.1E-09	1.6E-09	1.8E-07	9.8E-09	9.8E-07	2.5E-06	4.3E-05	9.6E-06	0.0E+00	0.0E+00	0.0E+00	0.0E+00							
0.0E+00	0.0E+00	0.0E+00	0.0E+00	0.0E+00	2.0E-09	0.0E+00	2.0E-09	0.0E+00	1.3E-08	8.0E-08	1.8E-07	1.5E-06	2.2E-06	2.0E-06	2.1E-05	3.2E-06	0.0E+00	0.0E+00	0.0E+00
0.0E+00	2.7E-09	2.0E-07	5.4E-08	1.0E-06	4.0E-06	7.4E-06	4.4E-06	1.6E-05	1.5E-05	0.0E+00	0.0E+00								
0.0E+00	7.0E-09	0.0E+00	1.7E-07	2.2E-07	1.2E-06	4.6E-06	3.0E-06	1.0E-06	9.5E-06	1.8E-05	4.5E-05	0.0E+00							
0.0E+00	1.3E-07	4.3E-07	1.2E-07	7.0E-07	6.5E-05	5.5E-05	1.1E-04	1.1E-04	1.0E-04	4.5E-04	1.1E-03								

Table 9: Absolute percent difference between MCNP and OpenMC. Scattering coefficients below 1.0E-5 are left to zero due to statistical error

3.2E+00	5.5E+00	5.2E+00	0.0E+00																
3.1E+00	1.4E+00	1.1E+01	0.0E+00																
1.2E+01	8.8E+00	2.6E+00	1.2E+01	0.0E+00															
0.0E+00	1.5E+00	1.4E-01	3.3E-01	1.3E+00	0.0E+00														
0.0E+00	0.0E+00	1.4E+00	5.6E-01	1.7E-02	2.3E+00	0.0E+00													
0.0E+00	0.0E+00	0.0E+00	1.6E+00	1.7E+00	4.4E-01	3.4E+00	0.0E+00												
0.0E+00	0.0E+00	0.0E+00	0.0E+00	0.0E+00	7.8E+00	1.7E+00	1.7E+01	0.0E+00											
0.0E+00	0.0E+00	0.0E+00	0.0E+00	0.0E+00	0.0E+00	1.3E+01	2.4E+00	3.6E+00	0.0E+00										
0.0E+00	3.9E-02	2.6E-02	0.0E+00																
0.0E+00	3.9E-02	1.3E-02	0.0E+00																
0.0E+00	2.7E-02	1.0E-02	0.0E+00																
0.0E+00	4.1E-02	1.7E-03	0.0E+00																
0.0E+00	6.3E-02	1.4E-02	0.0E+00																
0.0E+00	1.3E-02	9.9E-03	0.0E+00	0.0E+00	0.0E+00	0.0E+00	0.0E+00	0.0E+00											
0.0E+00	1.4E+00	2.5E-02	2.2E-02	0.0E+00	0.0E+00	0.0E+00	0.0E+00	0.0E+00											
0.0E+00	1.9E-01	8.1E-02	8.9E-02	6.9E-03	0.0E+00	0.0E+00	0.0E+00	0.0E+00											
0.0E+00	3.3E-01	5.5E-02	7.5E-02	5.4E-02	3.1E-03	0.0E+00	0.0E+00	0.0E+00											
0.0E+00	3.8E-01	1.3E-01	2.5E-01	1.4E-01	3.7E-02	1.6E-02	0.0E+00	0.0E+00											
0.0E+00	5.2E-01	1.8E-01	1.2E-01	3.8E-02	3.6E-01	4.8E-02	5.3E-02	0.0E+00											
0.0E+00	2.1E-01	2.7E+00	2.8E+00	2.2E+00	1.5E+00	2.1E+00	1.9E+00	2.2E+00											

### 3.8 Fission Neutron Spectra (FNS) Tally Comparison

The final tally for comparison is the Fission neutron spectra (FNS) tally. This provides both prompt and delayed fission spectra for the fuel system. After completing the runs, it became apparent that MCNP fixes the delay neutron time bins to the U235 6-group delay values. This reactor system is dominated by U235 fission and does not use plutonium or other fissile isotopes with significant impact on results. Alternative validations may require adjustment of the half-life bins to avoid discrepancies in the time bins values chosen.

Also, the FNS tally is different than the approach from OpenMC. OpenMC provides normalized fission spectra for each delay group and outputs delayed neutron fractions to match. MCNP builds the neutron fraction physics into the final results. The delay group tallies sum to the total fraction of neutrons from that time bin. Prompt fractions sum to around 99.3% and all six delayed bins sum to approximately 0.7% of fission neutrons which is consistent with most delayed neutron fractions for U235. Back-calculation from MCNP results can provide the delayed neutron fractions for each time bin and an effective beta for the whole system. Though not completed in this analysis, a simple KOPTS card in the MCNP deck could provide the beta effective to compare to the tally results.

MCNP provides an output spectrum at each energy bin. This is somewhat convoluted and unclear why this approach was used. This approach produces 20 different prompt spectra. Three MCNP prompt spectra were plotted in Figure 29. The results vary slightly between each energy group tally, but not enough to explain a separate physics being employed. At 20 energy groups and 1 prompt + 6 delay bins, 140 tally bins should be expected, but MCNP provides 20x20x7 where the first bin is prompt. Further explanation of this approach should be provided by MCNP developers. The results in Figure 29 show that three MCNP prompt spectra and the OpenMC prompt fission spectra are nearly identical and in excellent agreement.

The FNS tally also provides the delayed group data. When normalized, the delayed spectra are all similar in spectra with slight variations at higher energies. The OpenMC plots for each of 6 groups are plotted in Figure 30. It's clear from these tallies that a much finer binning at high energies could prove useful for comparison as the 20-group bins do not focus on the high energy neutrons. For deterministic transport applications, the fast flux groups tend to be coarsened as seen here. A more refined energy binning would be useful for comparison here but perhaps unnecessary in deterministic transport applications where some reactors are neutronicly dominated by thermalized flux. Figure 31 gives a direct comparison of delayed bins 1 and 6 between MCNP and OpenMC. The results are visually identical except for a very slight variation at the 2-5 MeV mark.

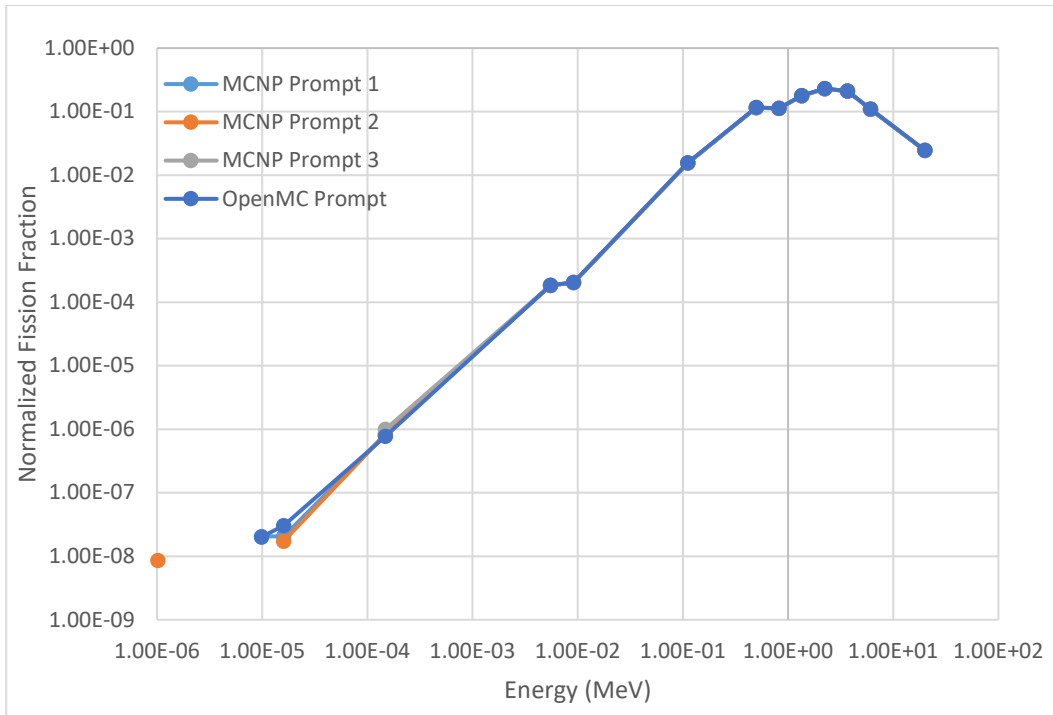


Figure 79: Prompt Fission Comparison. MCNP outputs multiple prompt results from FNS tally

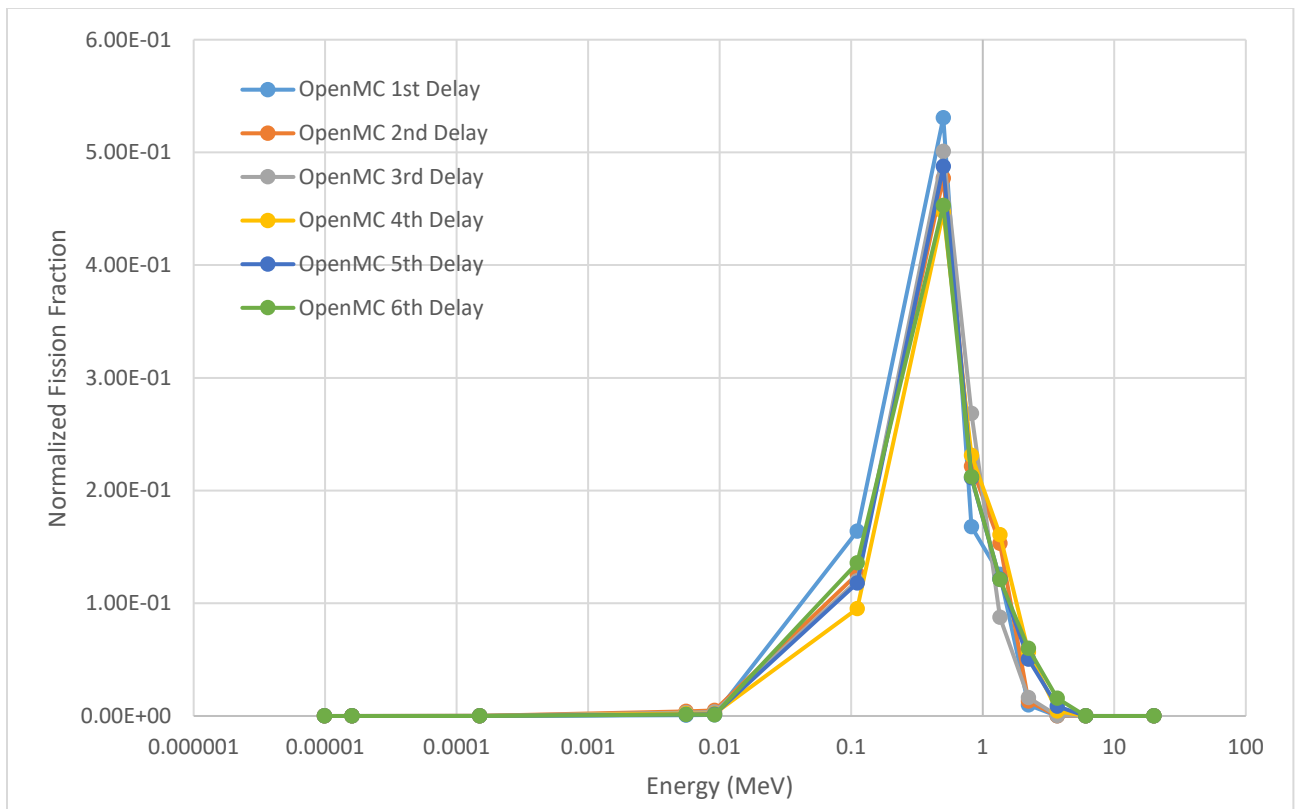


Figure 80: OpenMC Delayed Neutron Spectra for Snowflake assembly

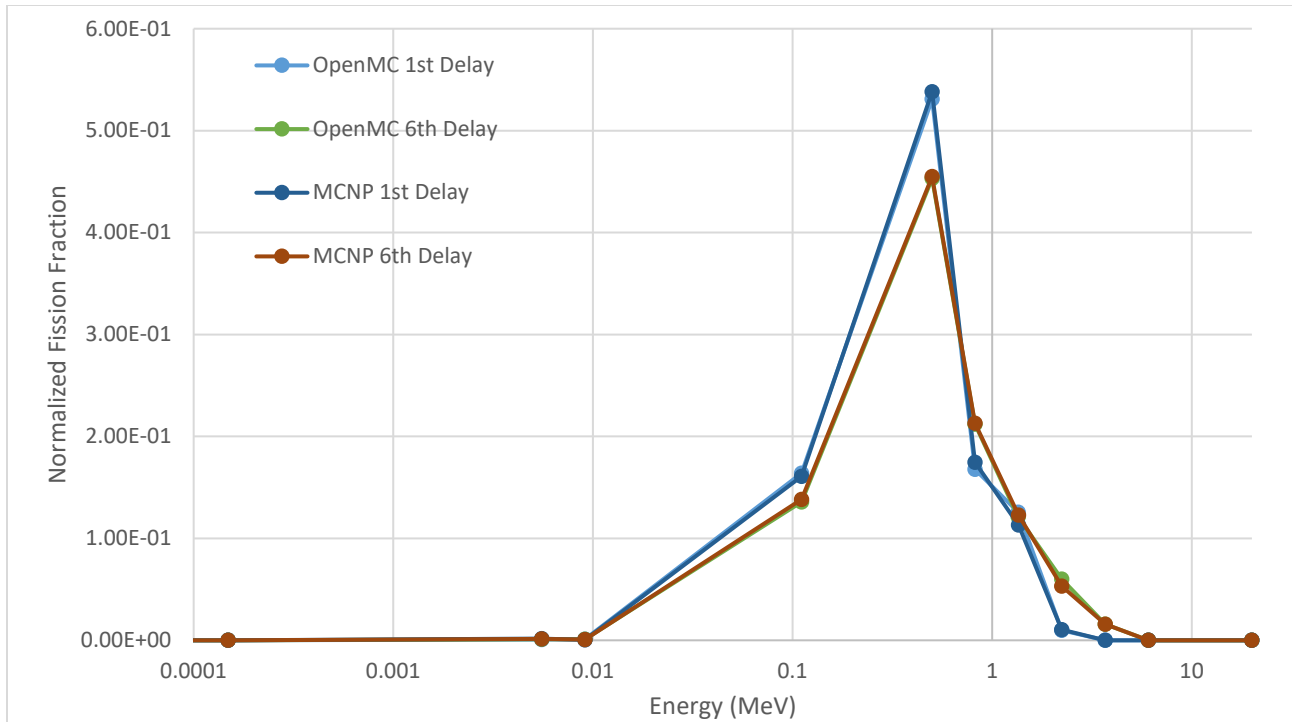


Figure 31: 1st and 6th Delayed Group Comparison between MCNP and OpenMC.

### 3.9 MCNP-OpenMC Reactor Comparison Summary

The results conclude that there is good agreement when using the same methodology for the cross section in MGC. In the MGC tally, the total, fission, and neutron velocity tallies show good agreement in all but the most thermal group which varies between the tools. It is unknown why such variation occurs in the thermal group, but as discussed, could be the methodologies of each tool. The default OpenMC and MCNP values may play a role in the calculation's thermal scatter group. Also, a slight variation is shown in an epi-thermal area. This occurs in a resonance area which may cause a discrepancy between the two tools. The kappa-fission results are implemented with different methodologies. Based on the kappa-fission data, the results indicate that kappa is being calculated different between the two tools. They systematically differ by around 12-15 MeV where MCNP has the lower kappa values. In terms of fission products, MCNP is not counting certain decay or delay products where OpenMC deposits everything but neutrinos. The neutron velocities are within 2% for each tool. The thermal group velocities do not suggest a more thermalized spectra in OpenMC to explain its higher cross sections. Overall, MGC is still generating results less than 4% between the tools. The scattering coefficient matrix also shows good agreement. Statistical uncertainty is evident but expected. The results for in-group scattering are within 3% between tools. The downscatter and upscatter results can vary up to 17% when the scattering cross sections are above  $1.0E-5$ . Because these in-group results are fairly close, the scattering cross section from MGC must also be fairly accurate between each tool. The FNS tally shows excellent agreement between prompt and delayed results. Very small variations are seen between the tools even with U235 fixed time bins in MCNP. Automatic weighting of the six group time bins should be implemented to remove the default U235 selection of time bins going forward. Also, diffusion coefficients and transport cross sections are

two desired values to calculate going forward for deterministic transport methods. Each tally comparison here shows proper working order for a non-trivial geometry. This provides confidence that the implementation into MCNP was correct with small variations more likely due to transport methods.

#### Acknowledgements

The authors would like to thank Wim Haeck and Nathan Gibson from the XCP-5 nuclear data team for providing assistance with NJOY calculations, including the input setup, code modifications and postprocessing of the multigroup data.

#### References

- [1] R. MacFarlane, D. W. Muir, R. M. Boicourt, A. C. Kahler, J. L. Conlin, "The NJOY Nuclear Data Processing System, Version 2016," Los Alamos National Laboratory Report, LA-UR-17-20093 (2017).
- [2] Paul K. Romano, Nicholas E. Horelik, Bryan R. Herman, Adam G. Nelson, Benoit Forget, and Kord Smith, "OpenMC: A State-of-the-Art Monte Carlo Code for Research and Development," *Ann. Nucl. Energy*, 82, 90--97 (2015).

## Appendix A

### MCNP model input listing

Pu model for NJOY/MCNP-MG comparison

1 100 0.04 -10 imp:n=1

2 0 10 imp:n=0

10 so 5.0

kcode 4000000 1.0 50 300

sdef pos=0 0 0 rad=d1

si1 0 5.0

sp1 -21 2

c

c xs and material cards

c

xs1 94239.10c 236.998600 94239.10c . 1 1 1041647 0 0 2.530E-08 ptable

m100 94239.10c 1

c

c tallies, including weighting spectrum

c

fc4 Weighting function for NJOY

f4:n 1

e4 1e-11 39998ilog 20

c

fc14 MG cross sections

f14:n 1

ft14 mgc

e14 1e-11 49ilog 20.

c

fc24 Scattering matrices

f24:n 1

ft24 spm 20

e24 1e-11 49ilog 20.

c

fc34 Legendre coefficient

f34:n 1

ft34 lcs 8

e34 1e-11 49ilog 20.

c

fc44 Fission neutron spectra

f44:n 1

ft44 fns 6

e44 1e-11 49ilog 20.

c

prdmp 2j 1 \$ Produce MCTAL file

## Appendix B

NJOY Input Listing (note text in >>> RED is not actually part of input file)

```
moder
 20 -30
reconr
-30 -21/
'PU239'/
9437 0/
.001/
0 /
broadr
-30 -21 -22/
9437 1 0 0/
.001/
293.6/
0/
heatr
-30 -22 -21/
9437 7/
302 303 304 318 402 443 444/
heatr
-30 -21 -23 24/
9437 7 0 1 0 2/
302 303 304 318 402 443 444/
thermr
0 -21 -22/
0 9437 20 1 1 0 0 1 221 0/
293.6/
0.001 10./
purr
-30 -22 -21/
9437 1 1 20 4/
293.6 /
1.e10 /
0/
gaspr
-30 -21 -22
groupr
-30 -22 0 45
9437 1 0 1 5 1 1 1 /
'PU239'
293.6
1e+10
50 /
1.000000e-05 1.762060e-05 3.104850e-05 5.470940e-05 9.640120e-05
```

1.698650e-04 2.993120e-04 5.274050e-04 9.293190e-04 1.637520e-03  
2.885400e-03 5.084250e-03 8.958750e-03 1.578580e-02 2.781560e-02  
4.901270e-02 8.636340e-02 1.521770e-01 2.681460e-01 4.724890e-01  
8.325530e-01 1.467010e+00 2.584960e+00 4.554850e+00 8.025910e+00  
1.414210e+01 2.491930e+01 4.390930e+01 7.737070e+01 1.363320e+02  
2.402250e+02 4.232910e+02 7.458630e+02 1.314260e+03 2.315800e+03  
4.080570e+03 7.190210e+03 1.266960e+04 2.232460e+04 3.933720e+04  
6.931450e+04 1.221360e+05 2.152110e+05 3.792150e+05 6.682000e+05  
1.177410e+06 2.074660e+06 3.655680e+06 6.441530e+06 1.135040e+07  
2.000000e+07 /

0. 0. 0 0 1 39999

39999 1

>>>

>>> INSERT

>>> MCNP

>>> WEIGHTING

>>> SPECTRUM

>>> HERE

>>>

3/

3 259/

3 452/

3 455/

3 456/

5 18 'prompt chi'/

5 455 'delayed chi'/

6/

8/

0/

0/

acer

-30 -22 0 31 32

1 0 1 .10 /

'PU239' /

9437 293.6 /

/

/

acer

0 31 33 34 35

7 1 1 -1 /

'PU239' /

viewr

33 37

stop